

## Carbon-Oxygen Classical Novae are Galactic <sup>7</sup>Li Producers as well as Potential Supernova Ia Progenitors

SUMNER STARRFIELD,<sup>1</sup> MAITRAYEE BOSE,<sup>2,3</sup> CHRISTIAN ILIADIS,<sup>4,5</sup> W. RAPHAEL HIX,<sup>6,7</sup> CHARLES E. WOODWARD,<sup>8</sup> AND R. MARK WAGNER<sup>9,10</sup>

<sup>1</sup>*Earth and Space Exploration, Arizona State University, P.O. Box 871404, Tempe, Arizona, 85287-1404, USA starrfield@asu.edu*

<sup>2</sup>*Earth and Space Exploration, Arizona State University, P.O. Box 871404, Tempe, Arizona, 85287-1404, USA*

<sup>3</sup>*Center for Isotope Analysis (CIA), Arizona State University, Tempe, Arizona, 85287-1404, USA*

<sup>4</sup>*Department of Physics & Astronomy, University of North Carolina, Chapel Hill, NC 27599-3255*

<sup>5</sup>*Triangle Universities Nuclear Laboratory, Durham, NC 27708-0308, USA*

<sup>6</sup>*Physics Division, Oak Ridge National Laboratory, Oak Ridge TN, 37831-6354*

<sup>7</sup>*Department of Physics and Astronomy, University of Tennessee, Knoxville, TN 37996*

<sup>8</sup>*MN Institute for Astrophysics, 116 Church Street, SE University of Minnesota, Minneapolis, MN 55455*

<sup>9</sup>*Large Binocular Telescope Observatory, Tucson, AZ 85721*

<sup>10</sup>*Department of Astronomy, Ohio State University, Columbus, OH 43210*

### ABSTRACT

We report on studies of Classical Nova (CN) explosions where we follow the evolution of thermonuclear runaways (TNRs) on Carbon Oxygen (CO) white dwarfs (WDs). We vary both the mass of the WD (from 0.6 M<sub>⊙</sub> to 1.35 M<sub>⊙</sub>) and the composition of the accreted material. Our simulations are guided by the results of multi-dimensional studies of TNRs in WDs that find sufficient mixing with WD core material occurs after the TNR is well underway, reaching levels of enrichment that agree with observations of CN ejecta abundances. We use NOVA (our 1-dimensional hydrodynamic code) to accrete solar matter until the TNR is ongoing and then switch to a mixed composition (either 25% WD material and 75% solar or 50% WD material and 50% solar). Because the amount of accreted material is inversely proportional to the initial <sup>12</sup>C abundance, by first accreting solar matter the amount of material taking part in the outburst is larger than in those simulations where we assume a mixed composition from the beginning. Our results show large enrichments of <sup>7</sup>Be in the ejected gases implying that CO CNe may be responsible for a significant fraction (~ 100 M<sub>⊙</sub>) of the <sup>7</sup>Li in the galaxy (~1000 M<sub>⊙</sub>). In addition, although the ejected gases are enriched in WD material, the WDs in these simulations eject less material than they accrete. We predict that the WD is growing in mass as a consequence of the accretion-outburst-accretion cycle and CO CNe may be an important channel of Supernova Ia progenitors.

### 1. INTRODUCTION

Classical Novae occur in close binary systems with a white dwarf (WD) primary and a secondary which is a larger cooler star that fills its Roche Lobe. It is losing material through the inner Lagrangian point which ultimately is accreted by the WD. These binary systems are referred to as Cataclysmic Variables (CVs). The consequence of the WD accreting sufficient material is a thermonuclear runaway (TNR) in matter that is electron degenerate at the beginning of accretion and thus produces an event that is designated a “nova outburst” (either Classical, Recurrent, or Symbiotic Nova; hereafter CN, RN, or SymN). While the observed outburst ejects material into the surrounding region, it does not disrupt the WD and continued accretion implies successive outbursts. In some cases, the properties of the WD and accretion result in outbursts repeated on human time-scales which are designated RNe. If the orbital separation is large and the secondary is a red giant, then the system is designated a SymN.

The observations of the chemical composition of the gases ejected by a CN explosion, show that they typically are extremely non-solar (Warner 1995; Gehrz et al. 1998; Bode & Evans 2008; Starrfield et al. 2012a; Downen et al. 2012). Because of the CNe observations, it is assumed that the accreting material mixes with the outer layers of the WD at some time during the evolution from the beginning of accretion to the observed outburst. Thus, the observed ejected gases consist of a mixture of WD and accreted material that has been processed by hot-hydrogen burning. It has also been assumed that the CN outburst ejects more mass (both accreted and WD matter) from the WD than accreted from the secondary star and, therefore, the WD is decreasing in mass as a result of continued CN outbursts and it

cannot be a progenitor of Supernova of type Ia (SN Ia). In contrast, if the WD accretes more mass than it ejects during the CN outburst, then it is growing in mass and could possibly reach the Chandrasekhar Limit and explode as a SN Ia. In this paper, we report on our new simulations of the CN outburst and find that the WD is ejecting less mass than accreted and, therefore, the WD is growing in mass and CO CNe could be one of the channels for the progenitors of SN Ia explosions.

SN Ia are the optically brightest explosions that occur in a galaxy and they can be detected to, at least,  $z \sim 2$  in the universe. Studies of SN Ia show that their light curves are standardizable, allowing them to be used as distance indicators, which led to the discovery of dark energy in the universe (Riess et al. 1998; Perlmutter et al. 1999). In addition, they contribute a significant fraction of the iron-group elements to the galaxy and the solar system (Hillebrandt & Niemeyer 2000; Leibundgut 2000). However, the systems that actually explode as a SN Ia are as yet unknown. Two pathways are currently posited, the single-degenerate (SD) and the double degenerate (DD). The DD scenario requires either the merging or collision of two carbon-oxygen (CO) WDs while the SD scenario assumes that a CO WD exists in a close binary stellar system and it is growing in mass toward the Chandrasekhar Limit (Hillebrandt & Niemeyer 2000; Leibundgut 2000, 2001; Maoz et al. 2014; Ruiz-Lapuente 2014; Polin et al. 2019). Therefore, the determination of the response of a CO WD to the CNe phenomenon (growing or shrinking in mass) may shed light on one channel of SN Ia progenitors.

Another important motivation for studies of the consequences of TNRs on CO WDs is the recent discovery of both  ${}^7\text{Li}$  and  ${}^7\text{Be}$  in the early high dispersion optical spectra of the ejected material from CN outbursts (Tajitsu et al. 2015, 2016; Izzo et al. 2015, 2018; Molaro et al. 2016; Selvelli et al. 2018; Wagner et al. 2018) which has validated earlier predictions (Starrfield et al. 1978; Hernanz et al. 1996; José & Hernanz 1998; Yaron et al. 2005) and warrants new theoretical studies. CNe produce  ${}^7\text{Li}$  via a process originally described by Cameron & Fowler (1971) for red giants. Starrfield et al. (1978) then applied their mechanism to CN explosions, but that version of NOVA did not, as yet, include accretion and they assumed that the envelope was already in place. Later Hernanz et al. (1996) and José & Hernanz (1998) followed the accreting material and were able to investigate the formation of  ${}^7\text{Be}$  during the TNR. They determined the amount of  ${}^7\text{Be}$  carried to the surface by convection and surviving before it could be destroyed by the  ${}^7\text{Be}(p,\gamma){}^8\text{B}$  reaction occurring in the nuclear burning region. If it survives by being transported to cooler regions,  ${}^7\text{Be}$  decays via electron-capture to  ${}^7\text{Li}$  with an  $\sim 53$  day half-life (Bahcall & Moeller 1969).

The studies reported in this paper confirm that a TNR on a CO WD overproduces  ${}^7\text{Be}$  with respect to solar material and in amounts that imply that such CNe are responsible for a significant amount of galactic  ${}^7\text{Li}$ . In contrast,  ${}^6\text{Li}$  is produced by spallation in the interstellar medium (Fields 2011) and its abundance in the solar system should not correlate with  ${}^7\text{Li}$ . Hernanz (2015) gives an excellent discussion of the cosmological importance of detecting  ${}^7\text{Li}$  in nova explosions. We return to this comparison in Section 5.1.

Here, we investigate both the SD scenario and the production of  ${}^7\text{Li}$  in the CN outburst by simulating accretion onto CO WDs, in which we include mixing of the WD outer layers with accreted solar matter after the TNR has been initiated. We report on three separate studies. First, we accrete mixed material (either 25% WD matter and 75% solar matter or 50% WD matter and 50% solar matter) from the beginning of accretion. This is the procedure used in the past for both accretion onto CO WDs and ONe WDs (Starrfield et al. 1997; José & Hernanz 1998; Starrfield et al. 2009; Hillman et al. 2014; Starrfield et al. 2016, and references therein). However, we find, as reported later, that these explosions do not agree with the observed aspects of CNe outbursts (Warner 1995; Starrfield et al. 2012a; Bode & Evans 2008). Second, we accrete solar matter from the beginning and follow the resulting evolution through the peak and the return to nuclear burning quiescence. Third, we take the solar accretion simulations and once the TNR is ongoing ( $T \sim 7 \times 10^7\text{K}$ ), we stop the evolution and switch the accreted layers to either of the mixed compositions noted above. This last set of simulations is guided by the results of multidimensional (Multi-D) studies of mixing on WDs which indicate that sufficient material is dredged up from the outer layers of the WD *during the TNR* to agree with observed abundances (Casanova et al. 2011b, 2016a, 2018; José 2014).

In the next section we discuss NOVA our 1-D hydrodynamic computer code. We follow that with the sections where we present the results for each of the above studies and end with a discussion and conclusions.

## 2. NOVA: OUR 1-DIMENSIONAL HYDRODYNAMIC CODE

We use NOVA (Kutter & Sparks 1972; Sparks & Kutter 1972; Kutter & Sparks 1974, 1980; Starrfield et al. 2009, 2016) in this study. The most recent description of NOVA can be found in Starrfield et al. (2009, and references therein). NOVA is a one-dimensional (1-D), fully implicit, hydrodynamic, computer code that has been well tested

against standard problems (Kutter & Sparks 1972; Sparks & Kutter 1972). NOVA includes a large nuclear reaction network that includes 187 nuclei (up to  $^{64}\text{Ge}$  and including the *pep* reaction), the OPAL opacities (Iglesias & Rogers 1996), the Starlib nuclear reaction rates (Sallaska et al. 2013), the Timmes equations of state (Timmes & Arnett 1999; Timmes & Swesty 2000), and the nuclear reaction network solver developed by Hix & Thielemann (1999). NOVA also includes the Arnett et al. (2010) algorithm for mixing-length convection and the Potekhin electron degenerate conductivities described in Cassisi et al. (2007). These improvements have had the effect of changing the initial structures of the WDs so that they have smaller radii and, thereby, larger surface gravities compared to our previous studies. Finally, we also now include the possible effects of a binary companion (an extra source of heating at radii of  $\sim 10^{11}$  cm) as described by MacDonald (1980) which can increase the amount of mass lost during the last stages of the outburst.

In this study, we accreted material at a rate of  $1.6 \times 10^{-10} M_{\odot}\text{yr}^{-1}$  onto complete CO WDs (the structure extends to the WD center) with masses of  $0.6 M_{\odot}$ ,  $0.8 M_{\odot}$ ,  $1.00 M_{\odot}$ ,  $1.15 M_{\odot}$ ,  $1.25 M_{\odot}$ , and  $1.35 M_{\odot}$ . We chose this value of  $\dot{M}$  because it is the value used by Hernanz et al. (1996); José & Hernanz (1998), and Rukeya et al. (2017) and later we compare our results to their results. It is also the value used in our study of accretion onto ONe WDs (Starrfield et al. 2009). The assumed composition of the WD outer layers was 50%  $^{12}\text{C}$  and 50%  $^{16}\text{O}$ . Since  $^{12}\text{C} > ^{16}\text{O}$  and the ratio varies with depth, this can only be considered an approximate value (Althaus et al. 2010; José et al. 2016; Giammichele et al. 2018). In fact, it is the amount of  $^{12}\text{C}$  that strongly affects the evolution and not the C/O ratio. The basic properties of each WD initial model (luminosity, radius, and effective temperature) are given in the first 3 rows of Tables 1 and 2. In contrast to our previous studies, we use 150 mass zones with the zone mass decreasing from the center to the surface. The mass of the surface zone is  $\sim 2 \times 10^{-9}$  in units of the WD mass. This is much less than either the accreted mass or the amount of core material mixed up into the envelope. This low a mass decreases the maximum time step during the accretion phase (which although implicit is tied to the mass of the outer zone), but allows us to fully resolve the behavior of the simulations as the TNR occurs.

NOVA follows accretion through the peak of the TNR and the following decline in the temperature toward quiescence. It allows us to evolve the expanding outer layers and determine if they are ejected. We tabulate, as the ejected mass, the amount of material that is expanding both at speeds above the escape velocity and also has become optically thin. We do not remove any mass zones during the evolution as this reduces the numerical pressure on the zones below causing them to accelerate outward and also reach escape speeds. We find that even if the material is ejected, we can follow the mass zones until they have reached radii of a few times  $10^{12}\text{cm}$ . At these radii the density in the outer layers has fallen to values that are now below the lower limit of the physics (opacity, pressure equation of state, energy equation of state) tables ( $\rho < 10^{-12} \text{ gm cm}^{-3}$ ) and we end the evolution.

Finally, although it is commonly assumed that a CO WD should not have a mass exceeding  $\sim 1.15M_{\odot}$  (Iben 1991; Ritossa et al. 1996; Iben et al. 1997), as we report in this paper our simulations suggest that WDs are growing in mass, so that there should be massive CO WDs in CN systems. An example of this class is Nova LMC 1991, a CO nova, which exhibited a super Eddington luminosity for more than 2 weeks (Schwarz et al. 2001) likely requiring a WD mass exceeding  $\simeq 1.35M_{\odot}$ . Moreover, the WDs in four of the nearest CVs (U Gem:  $1.2 M_{\odot}$  (Echevarría et al. 2007), SS Cyg:  $0.8 M_{\odot}$  (Sion et al. 2010), IP Peg:  $1.16 M_{\odot}$  (Copperwheat et al. 2010), and Z Cam:  $0.99 M_{\odot}$  (Shafter 1983)) are more massive than the canonical value for single WDs of  $0.6 M_{\odot}$  (Sion 1986). More recently, Sion et al. (2018) report a WD mass for the RN CI Aql of  $0.98 M_{\odot}$ , Shara et al. (2018) report that the mean WD mass for 82 Galactic CNe is  $1.13 M_{\odot}$  and 10 RNe is  $1.31 M_{\odot}$ , while Selvelli & Gilmozzi (2019) analyzed 18 old novae, using data from both IUE and Gaia, and report that many WDs in CNe have masses above the canonical value for single WDs.

### 3. SIMULATIONS WITH A MIXED COMPOSITION FROM THE BEGINNING

The principal motivation for this paper is to present a new set of simulations where we do not assume a mixed composition until the TNR is well underway. However, in order to demonstrate that there is a need for this technique, we first present the results of new simulations where we “Mix From the Beginning” (hereafter, MFB) as has been done in nova simulations for many years (Starrfield et al. 2016, and references therein). This technique was used because there was no consensus on how WD core matter was mixed into the accreted envelope although the observations of both fast CO and ONe CNe required that such mixing occur (Gehrz et al. 1998; Downen et al. 2012; Starrfield et al. 2016, and references therein). Nevertheless, it is not physically reasonable to assume the accreted matter is fully mixed from the beginning of accretion. A discussion of mixing mechanisms can be found in José et al. (2007).

We find that none of these MFB simulations eject sufficient material to agree with the observations and for those that do eject some material, the expanding gases have too low a velocity. This same result was also found in an earlier study of accretion onto CO WDs (Starrfield et al. 1997). In contrast, our previous ONe CNe simulations (Starrfield et al. 2009), which used the MFB technique, did eject significant material because they were initiated with a far lower value for the initial abundance of  $^{12}\text{C}$  and more material was accreted prior to the TNR than in the CO simulations.

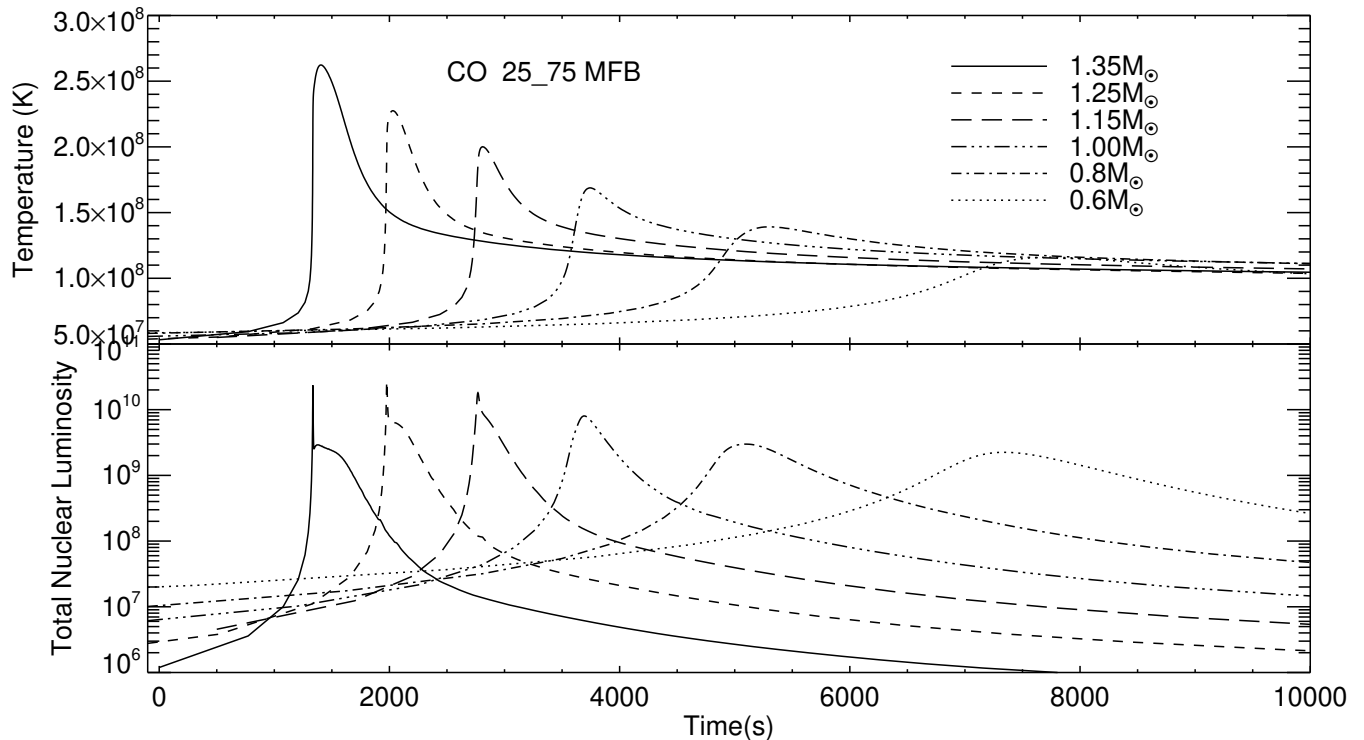


**Figure 1.** Top panel: the variation with time of the temperature in those mass zones near the interface between the outer layers of the CO WD and the accreted plus WD matter for the simulations with 25% WD material and 75% solar material. In these simulations we accreted the mixed composition from the beginning (MFB). The results for all six simulations are shown (the WD mass is identified in the legend). The curve for each sequence has been shifted in time to improve its visibility. As expected, the peak temperature achieved in each simulation is an increasing function of WD mass. Bottom panel: The variation with time of the total nuclear luminosity ( $\text{erg s}^{-1}$ ) in solar units ( $L_{\odot}$ ) around the time of peak temperature during the TNR. We integrated over all zones with ongoing nuclear fusion to obtain the plotted numbers. The identification with each WD mass is given on the plot and the evolution time has again been shifted to improve visibility. The cause of the sharp spike at the peak of the curve is discussed in the text.

We use two different mixed compositions in this study. The first is what we used in Starrfield et al. (1997) and is 50% WD matter and 50% solar matter (Lodders 2003). The second composition is 25% WD matter and 75% solar in order to better compare our results with Hernanz et al. (1996), José & Hernanz (1998), and Rukeya et al. (2017) who also investigated the consequences of 25% WD matter and 75% solar matter. In addition, Kelly et al. (2013) studied abundances in ONe novae and reported that the 25% WD - 75% solar mixture was a better fit to the observations.

The initial conditions and evolutionary results for the MFB simulations are given in Table 1. The columns are the values for each of the CO WD masses listed in the top row in solar mass. The first rows give the initial luminosity, radius, central temperature, central density, and effective temperature for each of the WD masses prior to accretion. As expected, as the WD mass increases, its radius decreases which is a result of electron degeneracy. We choose an initial luminosity of  $\sim 4 \times 10^{-3} L_{\odot}$  in order to obtain as large an amount of accreted mass as possible. This luminosity is the same value that we used in our ONe study (Starrfield et al. 2009) and only slightly smaller than the  $10^{-2} L_{\odot}$  used in José & Hernanz (1998). Increasing the initial luminosity does not change our conclusions; changing the initial chemical composition has a much larger effect. Since it is virtually the same initial luminosity for all the WD masses,

**Table 1.** Initial Parameters and Evolutionary Results for Accretion onto CO WDs: Mixing From Beginning (MFB)

| CO WD Mass ( $M_{\odot}$ ):   | 0.6   | 0.8               | 1.0               | 1.15              | 1.25              | 1.35              |
|---|-------|-------------------|-------------------|-------------------|-------------------|-------------------|
| Initial: $L/L_{\odot}(10^{-3})$                                       | 4.8   | 4.8               | 4.9               | 4.7               | 4.8               | 5.5               |
| Initial: $R(10^3\text{km})$   | 8.5   | 6.8               | 5.3               | 4.2               | 3.4               | 2.3               |
| Initial: $T_c(10^7\text{K})$  | 1.9   | 1.7               | 1.6               | 1.5               | 1.5               | 1.5               |
| Initial: $\rho_c(10^7\text{ gm cm}^{-3})$                             | 0.34  | 0.95              | 2.9               | 8.3               | 21.0              | 87.0              |
| Initial: $T_{\text{eff}}(10^4\text{K})$                               | 1.4   | 1.5               | 1.7               | 2.0               | 2.2               | 2.7               |
| <b>25% White Dwarf - 75% Solar</b>                                    |       |                   |                   |                   |                   |                   |
| $\tau_{\text{acc}}(10^5\text{ yr})$                                   | 9.8   | 3.8               | 2.0               | 1.0               | 0.6               | 0.2               |
| $M_{\text{acc}}(10^{-5}M_{\odot})$                                    | 15.5  | 6.0               | 3.1               | 1.7               | 0.9               | 0.3               |
| $T_{\text{peak}}(10^8\text{K})$                                       | 1.2   | 1.4               | 1.7               | 2.0               | 2.3               | 2.6               |
| $\epsilon_{\text{nuc-peak}}(10^{16}\text{erg gm}^{-1}\text{s}^{-1})$  | 0.014 | 0.041             | 0.20              | 0.89              | 2.4               | 6.1               |
| $L_{\text{peak}}/L_{\odot}(10^4)$                                     | 4.6   | 4.6               | 4.4               | 7.7               | 4.8               | 7.0               |
| $T_{\text{eff-peak}}(10^5\text{K})$                                   | 1.1   | 3.0               | 3.4               | 5.7               | 8.1               | 11.0              |
| $M_{\text{ej}}(10^{-7}M_{\odot})$                                     | 8.0   | 3.7               | 0.15              | 0.98              | 0.33              | 0.62              |
| $N(^7\text{Li}/\text{H})_{\text{ej}}/N(^7\text{Li}/\text{H})_{\odot}$ | 22.0  | $1.1 \times 10^2$ | $1.8 \times 10^2$ | $7.9 \times 10^2$ | $1.4 \times 10^3$ | $2.6 \times 10^3$ |
| $M_{\text{ej}}/M_{\text{acc}}(\%)$                                    | 0.5   | 0.6               | 0.05              | 0.6               | 0.4               | 2.0               |
| $V_{\text{max}}(10^2\text{km s}^{-1})$                                | 3.9   | 3.6               | 4.1               | 4.6               | 4.3               | 5.7               |
| <b>50% White Dwarf - 50% Solar</b>                                    |       |                   |                   |                   |                   |                   |
| $\tau_{\text{acc}}(10^5\text{ yr})$                                   | 6.1   | 3.2               | 1.6               | 0.8               | 0.5               | 0.2               |
| $M_{\text{acc}}(10^{-5}M_{\odot})$                                    | 9.7   | 5.0               | 2.5               | 1.3               | 0.7               | 0.2               |
| $T_{\text{peak}}(10^8\text{K})$                                       | 1.1   | 1.4               | 1.7               | 2.0               | 2.2               | 2.6               |
| $\epsilon_{\text{nuc-peak}}(10^{16}\text{erg gm}^{-1}\text{s}^{-1})$  | 0.015 | 0.081             | 0.33              | 1.4               | 4.3               | 17.0              |
| $L_{\text{peak}}/L_{\odot}(10^4)$                                     | 2.6   | 7.3               | 3.2               | 8.4               | 8.1               | 11.5              |
| $T_{\text{eff-peak}}(10^5\text{K})$                                   | 2.0   | 3.6               | 4.4               | 6.5               | 8.6               | 11.7              |
| $M_{\text{ej}}(10^{-7}M_{\odot})$                                     | 16.0  | 4.1               | 0.44              | 1.3               | 0.83              | 4.0               |
| $N(^7\text{Li}/\text{H})_{\text{ej}}/N(^7\text{Li}/\text{H})_{\odot}$ | 44.0  | $1.4 \times 10^2$ | $2.9 \times 10^2$ | $9.6 \times 10^2$ | $1.4 \times 10^3$ | $4.3 \times 10^3$ |
| $M_{\text{ej}}/M_{\text{acc}}(\%)$                                    | 1.6   | 0.8               | 0.2               | 1.0               | 1.2               | 20                |
| $V_{\text{max}}(10^2\text{km s}^{-1})$                                | 0.7   | 3.6               | 5.9               | 12.9              | 14.9              | 19.4              |

as the radius decreases the initial  $T_{\text{eff}}$  must increase. The decrease in radius, in turn, increases the gravitational potential energy at the surface and the TNR is reached with a smaller amount of accreted mass and, thereby, a smaller accretion time.

This can be seen in the next set of rows which give the evolutionary results for the first mixture which is 25% WD matter and 75% solar matter (Lodders 2003). (The composition is noted in “bold-face”). The rows are the accretion time to the beginning of the TNR,  $\tau_{\text{acc}}$ , and  $M_{\text{acc}}$  is the total accreted mass. The next set of rows tabulate, as a function of WD mass, the peak temperature in the simulation ( $T_{\text{peak}}$ ) with the scaling factor in parentheses for all rows, the peak rate of energy generation ( $\epsilon_{\text{nuc-peak}}$ ), the peak surface luminosity in units of the solar luminosity, ( $L_{\text{peak}}/L_{\odot}$ ), the peak effective temperature ( $T_{\text{eff-peak}}$ ), the amount of mass ejected in solar masses ( $M_{\text{ej}}$ ), the amount of  $^7\text{Li}$  ejected with respect to the solar value where we have assumed that all the  $^7\text{Be}$  produced in the TNR will decay to  $^7\text{Li}$ , ( $N(^7\text{Li}/\text{H})_{\text{ej}}/N(^7\text{Li}/\text{H})_{\odot}$ ), the ratio of the ejected mass to accreted mass in percent ( $M_{\text{ej}}/M_{\text{acc}}$ ), and the velocity of the surface zone which is the maximum velocity in each simulation ( $V_{\text{max}}$ ). We express the  $^7\text{Li}$  results in the same ratio as given by Hernanz et al. (1996, Table 1) so as to provide a direct comparison (see Section 5.1). Therefore, we use the Anders & Grevesse (1989) value for  $N(^7\text{Li}/\text{H})_{\odot}$  of  $2.04 \times 10^{-9}$  although in the simulations we use the Lodders (2003) abundance. The specific number does not matter in the simulations because all of the  $^7\text{Li}$  is destroyed by the TNR. In Table 3 (Section 5.1) we compare our  $^7\text{Li}$  and ejecta mass predictions with those of Hernanz et al. (1996);

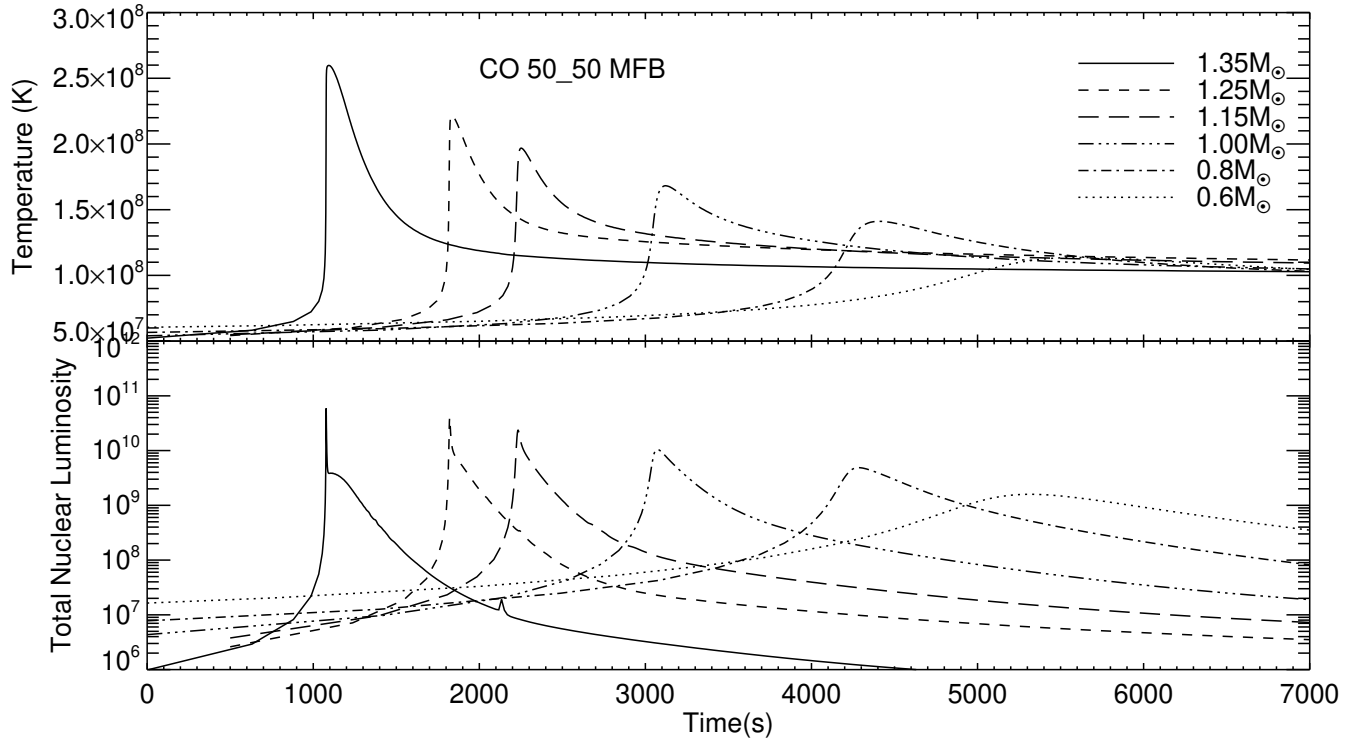


**Figure 2.** Top panel: The same plot as in Figure 1 but for the simulations with 50% WD matter and 50% solar matter and mixed from the beginning (MFB). While there is significantly more  $^{12}\text{C}$  in these simulations than in the 25% - 75% simulations, the increased energy production, once the CNO reactions have become important, results in less accreted mass and a smaller peak temperature. Again, we have shifted the curves in time to improve their visibility. Bottom panel: the same plot as shown in the bottom of Figure 1 but for the simulations with 50% WD matter and 50% solar. The small “glitch” in the  $1.35M_{\odot}$  sequence at a time of  $\sim 2100$  s is caused by a change in the spatial distribution of the region where nuclear burning is occurring.

José & Hernanz (1998), and Rukeya et al. (2017) who also mixed from the beginning. In Section 5.1 we also discuss the differences and agreements between our 3 studies.

In the following rows we tabulate exactly the same information but for the MFB simulations with 50% WD and 50% solar matter. Because of the increase in initial  $^{12}\text{C}$  abundance, once the accreting material gets sufficiently hot for CNO burning rather than the initial  $p-p$  chain, which now includes the  $pep$  reaction:  $p + e^{-} + p \rightarrow d + \nu$  as discussed in Starrfield et al. (2009), the increased energy generation per unit accreted mass reduces the time to the TNR and the amount of accreted mass. Interestingly, the peak temperature during the TNR is roughly the same for both mixtures. However, the peak rate of energy generation is considerably higher in the 50% WD - 50% solar mixture because of the increased  $^{12}\text{C}$  abundance. The remaining evolutionary parameters are also higher for the 50% WD - 50% solar mixture. The most material ejected at the highest velocities occurs for the 50% WD - 50% solar simulation on the  $1.35 M_{\odot}$  WD. However, the amount of ejected mass,  $4.0 \times 10^{-7} M_{\odot}$  is far lower than the typical ejecta mass estimates for CNe and so are the associated ejecta velocities (Warner 1995; Gehrz et al. 1998; Bode & Evans 2008; Starrfield et al. 2012a).

In the first three figures, we plot the evolutionary results for the MFB simulations. The top panel of Figure 1 shows the variation of temperature with time for the zone where peak conditions occur for all 6 CO WD masses. Our composition for these simulations is 25% WD - 75% solar matter, identified on the plot as 25.75 MFB. The WD mass is identified in the legend on the figure. We use the same line identifiers for WD mass in all the plots in this paper. As expected, the most massive WD reaches the highest peak temperature. We have offset each evolutionary sequence in time so as to clearly show the rise to maximum temperature and decline. The time axis is chosen to emphasize the major features in the evolution of each of the WD simulations. Peak temperature is reached a few hundred seconds after the increasing temperature exceeds  $10^8\text{K}$ . The rise in temperature ends when virtually all the light nuclei in the

convective region have become positron-decay nuclei ( $^{13}\text{N}$ ,  $^{14}\text{O}$ ,  $^{15}\text{O}$ , and  $^{17}\text{F}$ ) and no further proton captures can occur on  $^{14}\text{O}$  and  $^{15}\text{O}$  until they have decayed (Starrfield et al. 1972, 2016). The simulation for the  $0.6 M_{\odot}$  WD shows that the temperature has just reached the peak after 8000 s of evolution. We follow each of the simulations through peak temperature and its decline to values where no further nuclear burning is occurring in the outer layers.

Figure 2 shows the same two plots as in Figure 1 but for the composition with 50% WD matter and 50% solar matter (50\_50 MFB in the plots). Note the difference in the time axes between Figure 1 and Figure 2. As seen for both compositions, not only is the peak temperature an increasing function of WD mass, the rise and decay times are also functions of WD mass. For example in Figure 2, the rise time for the  $1.35 M_{\odot}$  WD is tens of seconds while that for the  $0.6 M_{\odot}$  WD is more than 4000 s.

The bottom panels of both Figure 1 and Figure 2 show the evolution of the total nuclear luminosity (in units of the solar luminosity) as a function of time for each composition. Again, the rise time for the most massive WDs is much shorter than for the lower mass WDs. Clearly, however, for these two compositions, the peak nuclear energy generation is nearly the same for the most massive WDs. The nuclear energy in the 50% WD - 50% solar simulations declines faster than in the 25% WD - 75% solar simulations because the ejection velocities are larger and the temperatures are dropping more rapidly. The sharp spike is characteristic of all our enriched carbon simulations. There is a steep rise to maximum nuclear luminosity as the expanding convective region encompasses more of the accreted layers, carrying the  $\beta^+$ - unstable nuclei to the surface. In addition, most of the CNO nuclei in the envelope are now  $\beta^+$ - unstable nuclei and any further rise in nuclear luminosity depends on these nuclei decaying. Their decay at the surface causes the peak energy generation in the surface mass zones to exceed  $10^{14} \text{ erg gm}^{-1}\text{s}^{-1}$  and results in an immediate expansion of the WD outer layers.

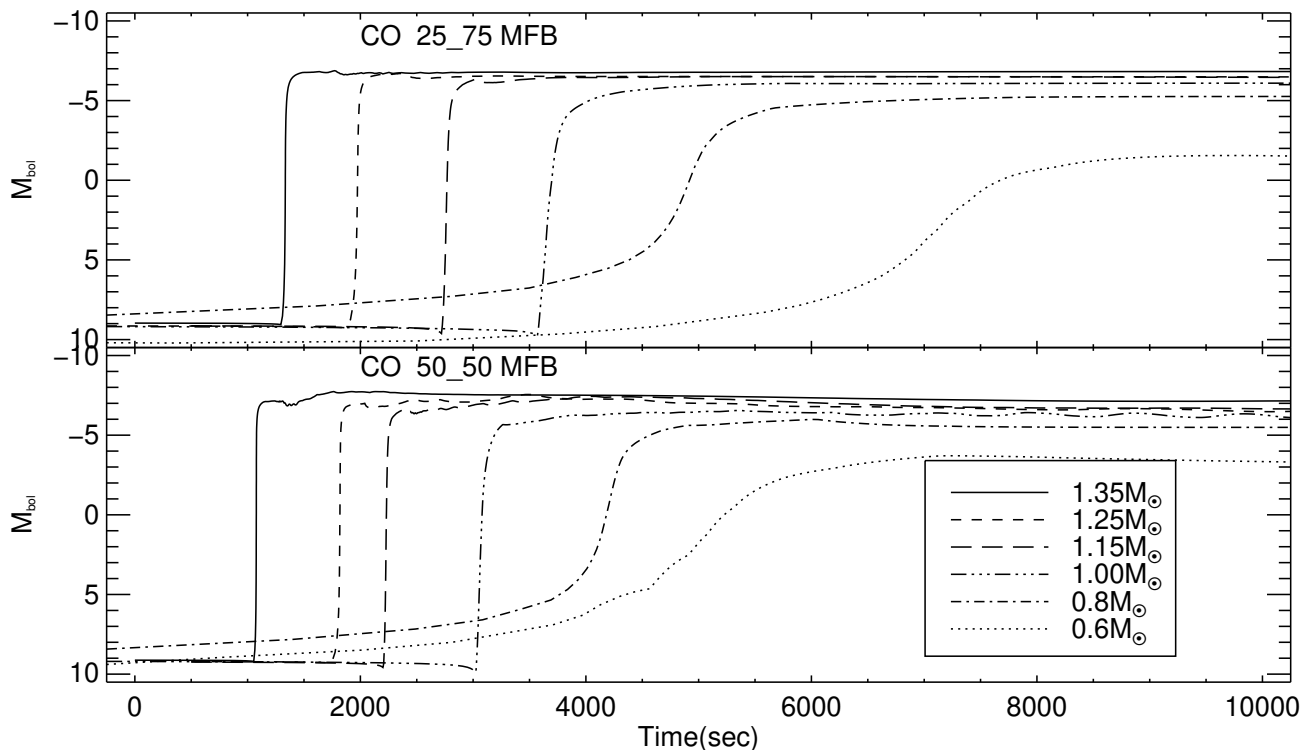


**Figure 3.** Top panel: the variation with time of the absolute bolometric magnitude for the simulations where we mixed a composition of 25% WD matter and 75% solar from the beginning (MFB). While the simulations on the more massive CO WDs reach values that agree with observations, those on the lower mass WDs are too faint to agree with the observations. Bottom panel: The same plot as in the top panel but for a mixed composition of 50% WD matter and 50% solar matter. Again the simulations on lower mass CO WDs do not reach to values that agree with typical CN observations where  $M_{\text{B,ol}}$  is around -7 or higher. The small variations are real and suggest oscillatory behavior in the light curves but these times are normally before the nova is discovered.

In Figure 3 we show the initial evolution of the bolometric magnitude as a function of time for both mixtures. The rapid rise to maximum is caused by the intense heat from the decays of the  $\beta^+$ -unstable nuclei that have reached the surface on the convective turn-over time ( $\sim 200$  s). In contrast, the absolute visual magnitudes for these simulations climb slowly in time as the expanding surface layers cool to  $\sim 10^4$  K. (They are not shown in order to prevent clutter in the figures.) The outermost zones reach this temperature when the surface radii have expanded to about  $10^{12}$  cm and we end the evolution. At this time the outermost layers have become optically thin and, if they have reached escape velocity, are expanding ballistically. We do not follow the simulations longer because the density in these layers has dropped below  $\sim 10^{-12}$  gm cm $^{-3}$ .

We note that attempts to predict the evolution of the light curve at later times typically use the Rosseland Mean which is a transparency mean (1/opacity) combined with a black-body source function. However, the atmospheres of CN after maximum do not resemble black-bodies.

We end this section by emphasizing that a key parameter affecting the evolution is the initial  $^{12}\text{C}$  abundance in the accreted material (Hernanz et al. 1996). This nucleus is a catalyst in the CNO cycle, and the MFB prescription implies a much higher initial  $^{12}\text{C}$  concentration than starting the simulation with just a solar composition. By increasing the amount of  $^{12}\text{C}$  with respect to hydrogen, once the CNO cycle becomes important, the rate of energy production is increased and the temperature in the nuclear burning region increases rapidly, per unit accreted mass, to the peak of the TNR. Thus, less mass is accreted than if the mixture had a solar composition (this is shown in Section 4.1). Reducing the amount of accreted mass at the time of peak temperature in the nuclear burning region, results in a lower density and temperature, and, thereby, less degeneracy. If the material is less degenerate, then it expands earlier in the TNR and, in combination with the formation of the  $\beta^+$ -unstable nuclei halts the rising temperature. Since the peak temperature is lower, the peak rate of energy generation is lower causing the total amount of energy produced during the TNR to be smaller. In consequence, too little mass is ejected, at too low velocities, and the properties of the simulations do not resemble typical CNe or RNe observations (Warner 1995; Bode & Evans 2008; Starrfield et al. 2012a).

#### 4. SIMULATIONS WITH THE COMPOSITION MIXED DURING THE THERMONUCLEAR RUNAWAY

As already emphasized, the treatment of the composition of the accreted material has changed in this study compared to our prior work. In our last study, we assumed that the mixing of WD and accreted material occurred from the beginning of the simulation and only used a composition of 50% WD (ONe) and 50% solar material (Starrfield et al. 2009). We began this study using this procedure but assumed a CO composition and found as reported both in Section 3 and previously in Starrfield et al. (1997, for a CO composition), that the results (ejected mass and ejecta velocities) were too small to agree with the observations.

In order to increase the amount of accreted material, therefore, we now use the results of multi-dimensional simulations as guides. These studies show that sufficient material is dredged-up into the accreted envelope from the outer layers of the WD by convectively associated instabilities when the TNR is well underway (Casanova et al. 2010a, 2011b, 2016b, 2018; José 2014). We simulate their calculations by first accreting a solar mixture (Lodders 2003) until the temperature in the nuclear burning region exceeds  $\sim 7.0 \times 10^7$  K and  $\sim 96\%$  of the accreted material is convective. At this time, we switch the composition of the accreted layers to a mixed composition (both abundances and the associated equations of state and opacities) and subsequently evolve the simulation through peak temperature and decline. It typically takes NOVA less than 2 s of “star” time (but many time steps) to adjust to the new composition. A similar technique has already been used by José et al. (2007) in their study of the “First Nova Explosions.” They explored a variety of time scales for mixing the WD material into the accreted layers, once convection was underway, and found that using short time scales was warranted. We choose an “instantaneous” time for mixing both because it is easily reproducible and because it is not in disagreement with their results.

##### 4.1. Solar Accretion

In this subsection, we present the evolution of just the solar accretion phase of the study. We then follow that with subsections describing the simulations assuming the mixed compositions. The initial conditions and evolutionary results are presented in Table 2. The variables in the tables are the same as already described for Table 1. The initial conditions for each of the 6 CO WD masses are given in the first 3 rows. The values in these rows are identical to the first 3 rows in Table 1 and are repeated here only for consistency. The next two rows give the accretion time to the beginning of the TNR,  $\tau_{\text{acc}}$ , and  $M_{\text{acc}}$  is the total accreted mass at that time. These values are those used both

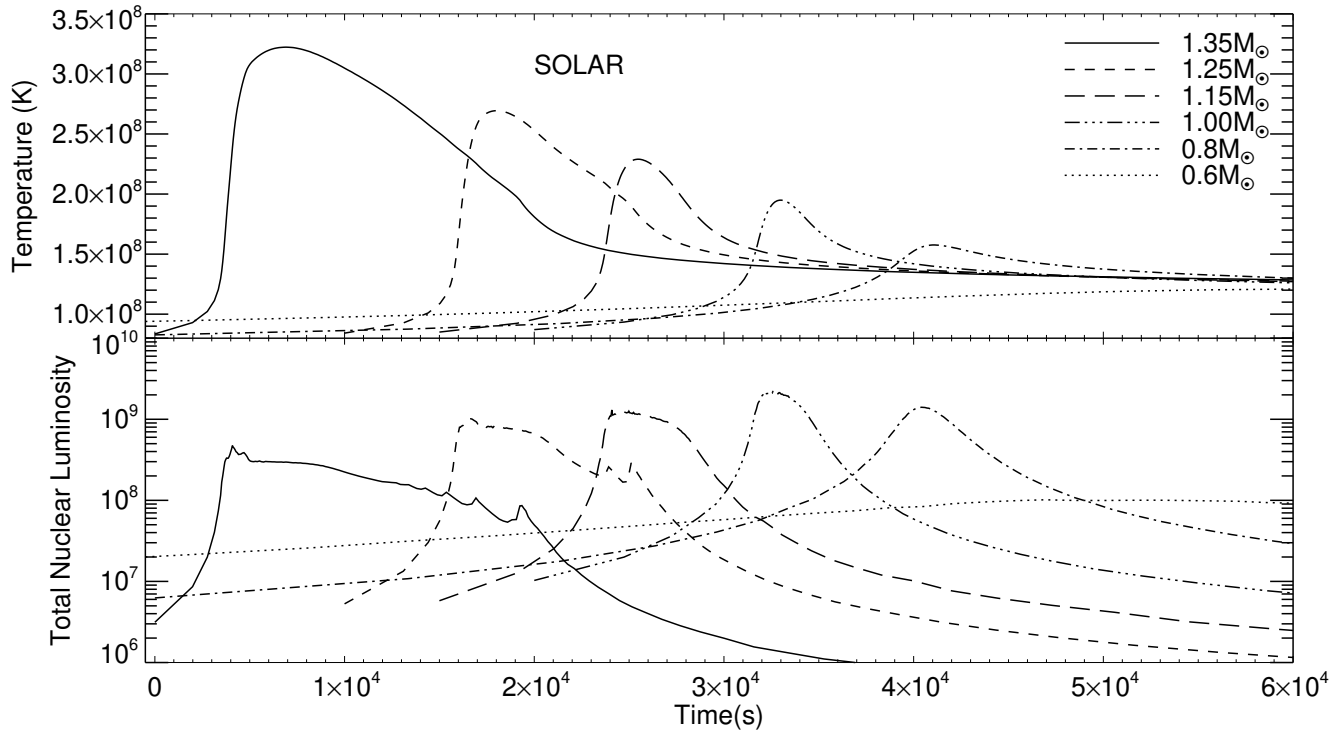


**Figure 4.** Top Panel: the same plot as in Figure 1 but for the simulations with accretion of only solar material. These simulations are used to determine the amount of mass accreted before switching to a mixed composition. Nevertheless, we follow them through the explosion. The time axis is much longer than for any of the other simulations because of the slow evolution of these sequences. Note that the  $0.6 M_{\odot}$  simulation has not yet reached peak temperature after  $5 \times 10^4$  s of evolution although it started from the same beginning temperature as the simulations for other CO WD masses. Bottom panel: the same plot as shown in the bottom panel of Figure 1 but for the simulations that accrete only solar matter and are assumed not to have mixed with WD matter. The “glitches” seen in the more massive WD evolution are caused by the convective region changing its spatial distribution, with respect to the mass zones, as the material expands. Unlike all the other simulations, the total energy increases as the WD mass decreases. This is because the accreted mass has declined with increasing WD mass and there is less material involved in the evolution. In contrast, both peak temperature and peak energy generation do increase with increasing CO WD mass as is shown in Table 2.

for the solar accretion simulations and, later, for the two mixed composition simulations for each of the listed WD masses (Section 4.2). We begin each of the sets of simulations with the composition listed in “bold-face”. As in the MFB simulations, we use 150 mass zones, with the mass of the zone decreasing outward in radius, and accrete at  $1.6 \times 10^{-10} M_{\odot} \text{ yr}^{-1}$ .

We can see the immediate effects of accreting a solar composition instead of a mixed composition. Comparing the results given in Table 2 to those in Table 1, the reduced amount of  $^{12}\text{C}$  in the solar accretion simulations significantly increases the amount of accreted mass. For example, comparing the solar accretion simulation to the 25% WD -75% solar (MFB) simulation, we find that about twice as much mass is accreted at  $0.6 M_{\odot}$  and a factor of 3 times more mass at  $1.35 M_{\odot}$ . Peak temperature is higher for all WD masses in the Solar accretion simulation as compared to the MFB simulations. The increased mass and degeneracy at the bottom of the accreted material clearly compensates for the larger amount of  $^{12}\text{C}$  in the MFB simulations.

Figure 4 (top panel) shows the evolution of the temperature with time for the zones where peak conditions in the TNR occur for all the CO WD masses accreting just a solar composition. Although there is more accreted mass in each of the simulations, the temperature evolution is extremely slow as shown by the time axis. While the  $1.35 M_{\odot}$  simulation takes  $\sim 2 \times 10^4$  s to evolve through the peak and decline of the TNR, the  $0.6 M_{\odot}$  simulation is still on the rise after  $\sim 5 \times 10^4$  s. In contrast, the equivalent MFB simulations take a far shorter time (shown in Figure 1 and Figure 2) to evolve through the peak as do the simulations to be reported on in the next subsection.

Figure 4 (bottom panel) shows the variation in total nuclear energy generation around the peak of the TNR. It should be compared with the bottom panels in Figures 1 and 2. The rise to peak nuclear energy generation is extremely slow and the decline is also slow. In addition, the peak is more than a factor of 10 lower than in the MFB simulations for the same WD mass. The “glitches” seen in the more massive WD evolution are caused by the convective region changing its spatial distribution, with respect to the mass zones, as the material expands. Unlike all the other simulations, the total energy as a function of time increases as the WD mass decreases. This is because the total accreted mass has declined with increasing WD mass and there is less material involved in the evolution. However, both peak temperature and peak energy generation do increase with increasing CO WD mass as is shown in Table 2.

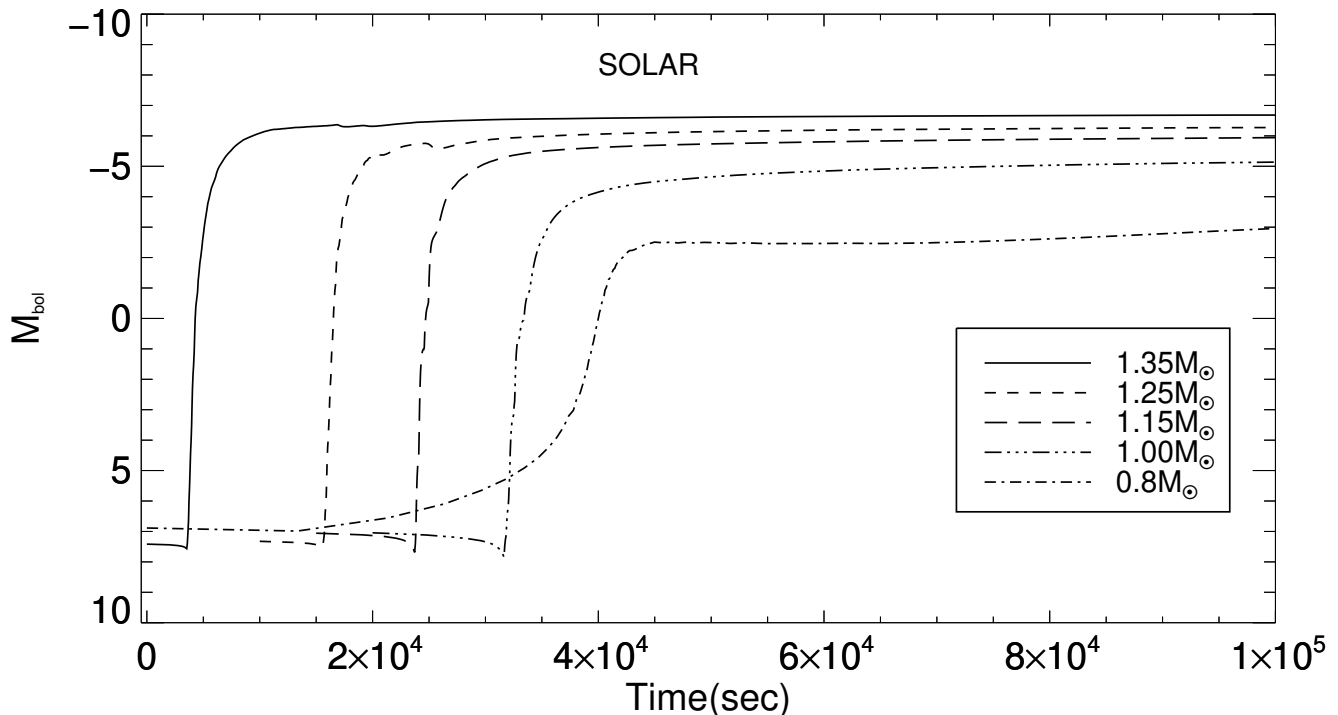


**Figure 5.** The same plot as shown in Figure 3 but for the solar composition simulations. Note that only the simulations on the most massive CO WDs reach peak values close to those that are observed. They also evolve extremely slowly compared to the mixed compositions (both MFB and MDTNR) as can be seen on the time axis. We do not plot the evolution of the  $0.6 M_{\odot}$  simulation since it is still rising after  $10^5$ s.

Figure 5 is the solar accretion analog of Figure 3, showing the time evolution of the bolometric magnitude for the solar accretion simulations. Peak  $M_{\text{bol}}$  is an increasing function of WD mass but even the simulation on the most massive WD does not reach values that are observed in a typical CN outburst of  $\sim -8$ . These, however, might fit some of the slowest and faintest CNe shown in Kasliwal et al. (2011).

Alternatively, mixing may occur in these CNe but, if the outer layers of the WD consist of material that has undergone previous CN outbursts, and the outburst has left a helium enriched layer behind, it will be helium enriched material that is mixed into the accreted layers in addition to  $^{12}\text{C}$  enriched material. In fact, spectroscopic studies of CNe ejecta show that this material is strongly enriched in helium and to amounts that suggest that helium has been mixed up from below and is not just the residue of the hot-hydrogen burning reactions that drove the TNR.

Finally, we note that the consequences of accretion of solar material onto WDs with a larger variation in mass and mass accretion rates, and where **no** mixing of WD with accreted material was assumed, has been published elsewhere (Starrfield et al. 2012a,b; Newsham et al. 2014). They found that a TNR occurred for all WD masses and mass accretion rates.

#### 4.2. The Simulations using Compositions Mixed During the TNR

**Table 2.** Initial Parameters and Evolutionary Results for Accretion onto CO WDs: Mixing During the Thermonuclear Runaway (MDTNR)

| CO WD Mass ( $M_{\odot}$ ):   | 0.6                  | 0.8                  | 1.0                  | 1.15                 | 1.25                 | 1.35                 |
|---|----------------------|----------------------|----------------------|----------------------|----------------------|----------------------|
| Initial: $L/L_{\odot}(10^{-3})$                                       | 4.8                  | 4.8                  | 4.9                  | 4.7                  | 4.8                  | 5.5                  |
| Initial: $R(10^3\text{km})$   | 8.5                  | 6.8                  | 5.3                  | 4.2                  | 3.4                  | 2.3                  |
| Initial: $T_{\text{eff}}(10^4\text{K})$                               | 1.4                  | 1.6                  | 1.8                  | 2.0                  | 2.2                  | 2.7                  |
| $\tau_{\text{acc}}(10^5 \text{ yr})$                                  | 19.8                 | 9.9                  | 5.1                  | 2.4                  | 1.6                  | 0.6                  |
| $M_{\text{acc}}(10^{-5}M_{\odot})$                                    | 31.4                 | 16.0                 | 8.1                  | 3.9                  | 2.6                  | 1.0                  |
| <b>Solar mixture</b>  |                      |                      |                      |                      |                      |                      |
| $T_{\text{peak}}(10^8\text{K})$                                       | 1.2                  | 1.6                  | 2.0                  | 2.3                  | 2.6                  | 3.0                  |
| $\epsilon_{\text{nuc-peak}}(10^{14}\text{erg gm}^{-1}\text{s}^{-1})$  | 0.032                | 0.73                 | 1.6                  | 1.8                  | 1.6                  | 1.8                  |
| $L_{\text{peak}}/L_{\odot} (10^4)$                                    | 3.9                  | 3.8                  | 2.1                  | 2.7                  | 3.2                  | 3.9                  |
| $T_{\text{eff-peak}}(10^5\text{K})$                                   | 0.9                  | 1.6                  | 2.0                  | 3.4                  | 5.3                  | 7.7                  |
| $M_{\text{ej}}(10^{-7}M_{\odot})$                                     | 6.8                  | 12.0                 | 0.034                | 0.33                 | 0.0                  | 0.30                 |
| $N(^7\text{Li}/\text{H})_{\text{ej}}/N(^7\text{Li}/\text{H})_{\odot}$ | $1.0 \times 10^{-5}$ | $1.4 \times 10^{-5}$ | $1.5 \times 10^{-2}$ | $4.7 \times 10^{-3}$ | $4.6 \times 10^{-4}$ | $6.2 \times 10^{-3}$ |
| $M_{\text{ej}}/M_{\text{acc}}(\%)$                                    | 0.2                  | 0.8                  | $\sim 0.0$           | $\sim 0.0$           | 0.0                  | 0.3                  |
| $V_{\text{max}}(10^2\text{km s}^{-1})$                                | 3.6                  | 4.5                  | 3.8                  | 5.1                  | 0.0                  | 4.8                  |
| <b>25% White Dwarf - 75% Solar</b>                                    |                      |                      |                      |                      |                      |                      |
| $T_{\text{peak}}(10^8\text{K})$                                       | 1.3                  | 1.7                  | 2.0                  | 2.4                  | 2.8                  | 3.4                  |
| $\epsilon_{\text{nuc-peak}}(10^{16}\text{erg gm}^{-1}\text{s}^{-1})$  | 0.66                 | 0.65                 | 1.2                  | 3.4                  | 11.4                 | 34.3                 |
| $L_{\text{peak}}/L_{\odot} (10^5)$                                    | 0.7                  | 8.5                  | 2.8                  | 2.3                  | 3.3                  | 7.3                  |
| $T_{\text{eff-peak}}(10^5\text{K})$                                   | 1.1                  | 2.4                  | 3.2                  | 8.4                  | 8.0                  | 10.5                 |
| $M_{\text{ej}}(10^{-6}M_{\odot})$                                     | 0.49                 | 2.9                  | 4.3                  | 12.8                 | 20.8                 | 4.6                  |
| $N(^7\text{Li}/\text{H})_{\text{ej}}/N(^7\text{Li}/\text{H})_{\odot}$ | 78.0                 | $5.0 \times 10^2$    | $1.6 \times 10^3$    | $2.8 \times 10^3$    | $3.0 \times 10^3$    | $3.5 \times 10^3$    |
| $M_{\text{ej}}/M_{\text{acc}}(\%)$                                    | 0.2                  | 2                    | 5                    | 33                   | 80                   | 46                   |
| $V_{\text{max}}(10^3\text{km s}^{-1})$                                | 0.4                  | 1.4                  | 2.8                  | 2.8                  | 3.4                  | 1.4                  |
| <b>50% White Dwarf - 50% Solar</b>                                    |                      |                      |                      |                      |                      |                      |
| $T_{\text{peak}}(10^8\text{K})$                                       | 1.4                  | 1.8                  | 2.2                  | 2.5                  | 3.4                  | 4.3                  |
| $\epsilon_{\text{nuc-peak}}(10^{17}\text{erg gm}^{-1}\text{s}^{-1})$  | 0.012                | 0.085                | 0.47                 | 1.7                  | 26.0                 | 298.0                |
| $L_{\text{peak}}/L_{\odot} (10^6)$                                    | 3.0                  | 2.6                  | 3.4                  | 2.0                  | 2.7                  | 3.9                  |
| $T_{\text{eff-peak}}(10^5\text{K})$                                   | 1.5                  | 3.2                  | 4.2                  | 8.3                  | 8.3                  | 43.0                 |
| $M_{\text{ej}}(10^{-5}M_{\odot})$                                     | 16.0                 | 11.0                 | 6.3                  | 3.4                  | 2.3                  | 0.86                 |
| $N(^7\text{Li}/\text{H})_{\text{ej}}/N(^7\text{Li}/\text{H})_{\odot}$ | $1.9 \times 10^2$    | $7.4 \times 10^2$    | $1.6 \times 10^3$    | $2.8 \times 10^3$    | $3.6 \times 10^3$    | $3.4 \times 10^3$    |
| $M_{\text{ej}}/M_{\text{acc}}(\%)$                                    | 51                   | 69                   | 78                   | 87                   | 90                   | 88                   |
| $V_{\text{max}}(10^3\text{km s}^{-1})$                                | 2.5                  | 4.3                  | 6.4                  | 6.6                  | 6.5                  | 5.6                  |

We now take the results for each CO WD mass from the evolution reported in the last subsection and switch to a mixed composition when the peak temperature in the simulation has reached  $\sim 7.0 \times 10^7$  K and convection is well underway but has not yet reached the surface. Once we have switched the composition, we continue the evolution, without assuming any further accretion, through peak temperature of the TNR and the following decline in temperature to where there is no further nuclear burning in the outer layers. We use the same two mixtures (either 25% WD and 75% solar material or 50% WD and 50% solar material) as used in the MFB simulations. These two sets of simulations are identified on the plots as either 25.75 Mixing During the TNR (25.75 MDTNR) or 50\_50 Mixing During the TNR (50\_50 MDTNR).

We emphasize that the same *initial* model (thermal structure, spatial structure, and amount of accreted mass distributed through the same number of mass zones) is used for the two sets of simulations at the time we switch to a mixed composition. The violence of the resulting evolution now depends on the amount of  $^{12}\text{C}$  in the accreted

layers (solar plus WD) *after* the switch in composition. Since, for the same temperature and density, increasing the  $^{12}\text{C}$  abundance increases the rate of energy generation, the simulations evolve much more rapidly, and reach higher peak values than the equivalent MFB simulation (for the same WD mass and mixed composition). This result is in contrast to the previously described MFB accretion phases (Section 3) where a higher initial  $^{12}\text{C}$  abundance resulted in a weaker explosion. Peak temperature is reached about one hundred seconds after the temperature exceeds  $10^8\text{K}$ . The rise in temperature ends because virtually all the light nuclei in the convective region have become positron decay nuclei.

We follow each of the simulations through peak nuclear burning, peak temperature, and decline. We end the simulation when the outer layers have reached radii of  $\simeq \text{few} \times 10^{12}$  cm. At this radius they have started to become optically thin and, in some of the simulations, the material has reached escape velocity and the density has declined to below  $\sim 10^{-12}$  gm cm $^{-3}$ .

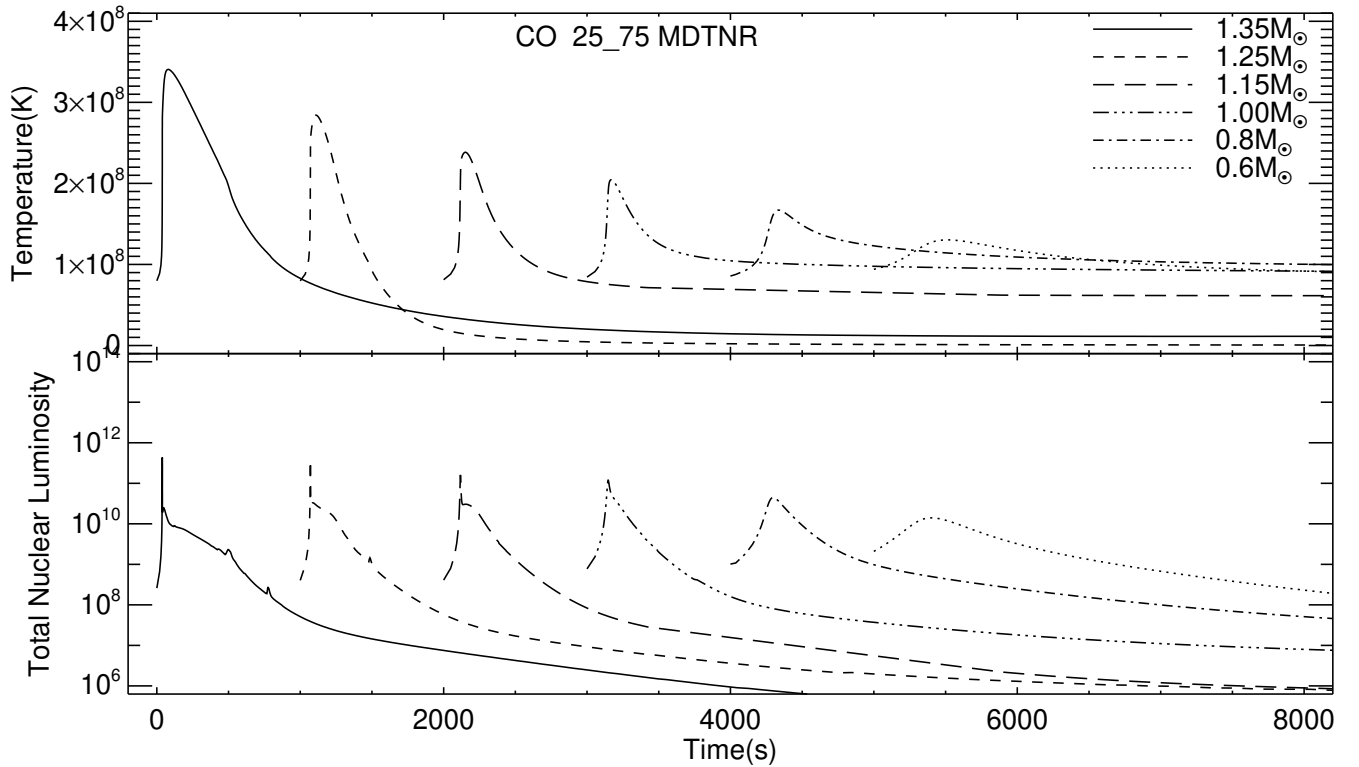


**Figure 6.** Top panel: the variation with time of the temperature in those mass zones near the interface between the outer layers of the WD and the accreted plus WD matter for the simulations with 25% WD material and 75% solar. This plot is the analog of the top panel of Figure 1. The results for all six simulations are shown (the WD mass is identified in the inset). The curve for each sequence has been shifted in time to improve its visibility. As expected, the peak temperature achieved in each simulation is an increasing function of CO WD mass. Bottom panel: same as the bottom panel of Figure 1 but for the simulation with 25% WD-75% solar. The small “glitches” that appear on the decline are caused by convection moving in and out and bringing in small amounts of fresh nuclei to the nuclear burning regime.

As discussed in the last subsection, the first set of evolutionary results in Table 2 shows the consequences of following the solar accretion simulation through the TNR, without any mixing, and its return to near quiescence. The next two sets of rows provide exactly the same information but for the mixed composition simulations with 25% WD and 75% solar matter, and followed below by the results for the 50% WD and 50% solar matter simulations. Comparing the 25% WD-75% solar MDTNR simulations to the 50% WD-50% solar MDTNR simulations, the large enrichment of  $^{12}\text{C}$  in the simulations with more WD matter causes a more extreme set of evolutionary results.

The plots of temperature versus time for these two sets of simulations are given in Figures 6 and 7. Both the vertical and horizontal scales in these two figures are different. As noted before, the peak temperature during the TNR is an increasing function of WD mass. The simulation with 25% WD-75% solar MDTNR involving a CO WD with a

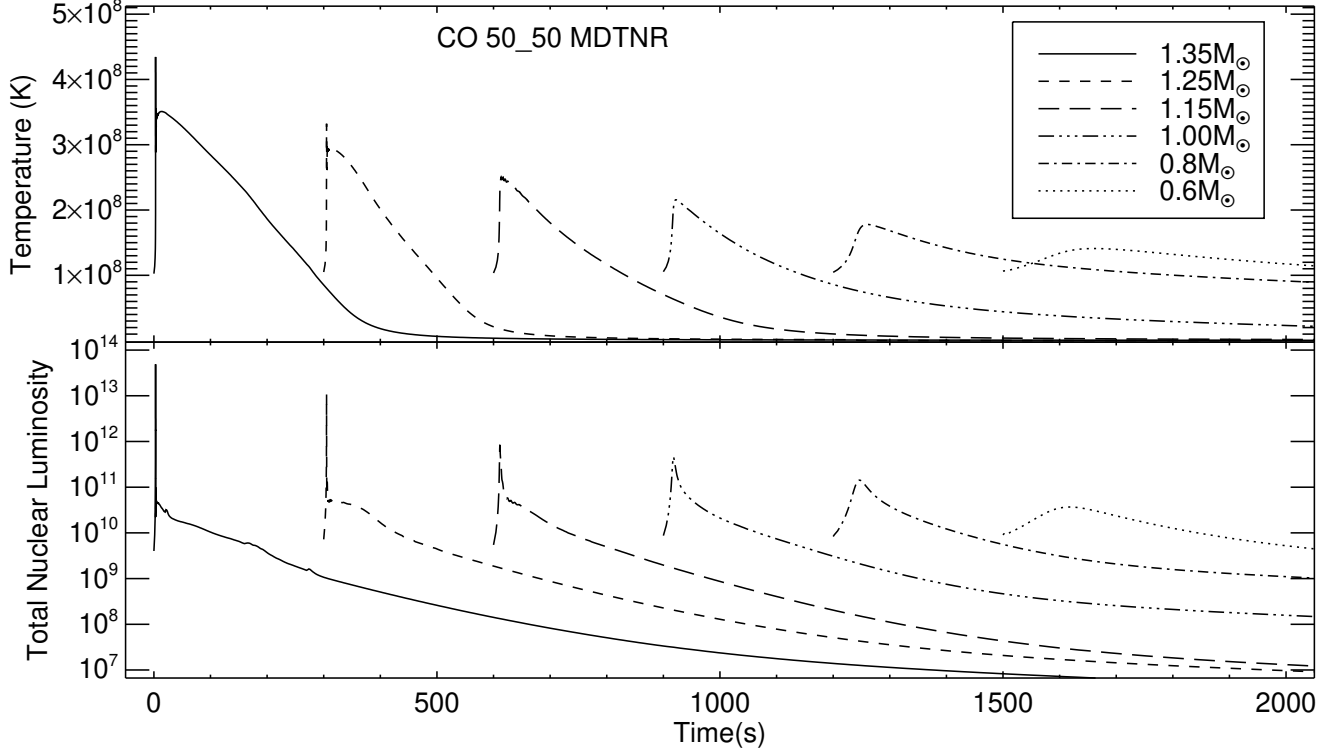


**Figure 7.** Top panel: same as Figure 6 but for the simulations with 50% WD matter and 50% accreted matter. Because of the increased  $^{12}\text{C}$ , the rate of energy generation is larger for a given temperature and density, and these simulations evolve much more rapidly than the simulations with a lower  $^{12}\text{C}$  abundance. Therefore, the evolution time for this series of sequences is significantly shorter than that in Figure 6. The extremely rapid increase and decrease in temperature indicate that the simulation formed a shock wave in the zone where peak temperature occurred. Bottom panel: the same plot as in Figure 6 but for the simulation with 50% WD matter and 50% accreted matter. Note that the horizontal and vertical axes differ in these two plots. Because of the much larger amount of  $^{12}\text{C}$  in these simulations, the evolution is more extreme and faster than for those simulations with a smaller amount of  $^{12}\text{C}$ .

mass of  $1.35 M_{\odot}$  reaches the highest temperature of  $3.4 \times 10^8$  K, while the simulation on the lowest mass WD,  $0.6 M_{\odot}$ , reaches the lowest peak temperature of  $1.3 \times 10^8$  K (Figure 6). Comparing these values to the results for the 50% WD-50% solar MDTNR simulations, we find that there is hardly any difference in peak temperature and energy generation for the lower mass WDs but the values for the  $1.25 M_{\odot}$  and  $1.35 M_{\odot}$  simulations are far larger for the more carbon enriched simulation (see Table 2 and Figure 7). The peak temperature for the  $1.35 M_{\odot}$  50% WD-50% solar MDTNR simulation reaches  $4.3 \times 10^8$  K and the peak rate of energy generation is  $3.0 \times 10^{19}$  erg  $\text{gm}^{-1}\text{s}^{-1}$  in the region closest to the interface between the WD core and accreted plus core material. The rise in temperature for this sequence is so rapid that a shock forms at the interface between the accreted and WD matter and moves through the envelope in seconds. The consequences of the shock can be seen in ejection velocities that exceed  $5,600 \text{ km s}^{-1}$  for the most massive WDs (Table 2). The sharp spike in the  $1.35 M_{\odot}$  50% WD-50% solar MDTNR simulation shows the shock formation. The luminosities and effective temperatures for the 50% WD- 50% solar MDTNR evolution exceed those for observed CNe explosions. We suggest that this mixture is too extreme.

Figures 6 (for the 25% WD-75% solar MDTNR simulations) and 7 (for the 50% WD-50% solar MDTNR simulations) also show (bottom panels) the variation with time of the total nuclear luminosity in solar units ( $L_{\odot}$ ) around the time of peak temperature. The glitches are caused by the spatial distribution of the convective region moving inwards and outwards and bringing in fresh partially burned material. Note that both the vertical and horizontal axes differ in these two plots. Both sets of simulations show an extremely rapid rise to maximum and a sharp decline followed by a slower decline. The step rise to maximum nuclear luminosity occurs as the convective region encompasses all the accreted layers thus carrying the  $\beta^+$ - unstable nuclei to the surface and unprocessed CNO nuclei down to the nuclear burning region.

As in the MFB evolutionary sequences, the rise time for the most massive CO WDs is shorter than for the lower mass CO WDs. However, for these two compositions, the peak nuclear energy generation is nearly the same for the massive WDs but decreases with decreasing WD mass for the lower mass WDs. In contrast, as shown in Figure 6 and Figure 7, the total nuclear luminosity decreases as the CO WD mass decreases. For all masses, the peak is higher for the 50% WD-50% solar MDTNR simulations. The extremely sharp spike for the  $1.35 M_{\odot}$  50% WD - 50% solar evolution indicates that a shock has formed. The nuclear energy in the 50% WD - 50% solar MDTNR simulations declines faster than in the 25% WD - 75% solar simulations because the expansion velocities are larger and, therefore, the temperatures drop more rapidly.

Table 2 shows that the peak luminosities and effective temperatures are much higher for the 50% WD - 50% solar MDTNR mixture and massive WDs. The peak luminosities for the 25% WD - 75% solar MDTNR simulations range from  $7 \times 10^4 L_{\odot}$  for the  $0.6 M_{\odot}$  WD to  $7.3 \times 10^5 L_{\odot}$  for the  $1.35 M_{\odot}$  WD, although the highest luminosity is  $8.5 \times 10^5 L_{\odot}$  for the  $0.8 M_{\odot}$  WD. These values are not unreasonable when compared to observations if we realize that CNe typically are discovered in outburst long after peak conditions occurred in the nuclear burning region and we have ended the evolution.

In contrast, the peak luminosities for the 50% WD - 50% solar MDTNR mixture range from  $2.0 \times 10^6 L_{\odot}$  to  $4.0 \times 10^6 L_{\odot}$  which are too high to agree with the observations. These high luminosities, in combination with the predicted effective temperatures which range from  $8.3 \times 10^5 K$  for the  $1.15 M_{\odot}$  simulation to  $4.3 \times 10^6 K$  for the  $1.35 M_{\odot}$  simulation, would trigger responses in some of the X-ray detectors currently in orbit. Such triggers have not occurred. However, the 25% WD-75% solar MDTNR simulation on a  $1.25 M_{\odot}$  WD reaches  $3.3 \times 10^5 K$  and that on a  $1.35 M_{\odot}$  WD reaches  $2.2 \times 10^5 K$  which are less than seen in the results of some of the X-ray grating studies of CN near the peak (Orion et al. 2018, and references therein) and suggest that mixtures between the two that we have studied might be in better agreement with the peak luminosity predictions.

Both Table 1 and 2 give the mass ejected by each of the simulations along with the ratio of ejected to accreted mass (in percent) as a function of CO WD mass. In Figure 8, we show the same data (the ratio of ejected to accreted mass in percent) as a function of WD mass for all the mixed sequences that we evolved. Clearly, less mass is ejected than accreted. The only sequences that eject a significant amount of material are the 50% WD - 50% solar MDTNR sequences on the most massive WDs. In contrast, the 25% WD - 75% solar sequences show that only the  $1.25 M_{\odot}$  sequence ejects a sufficient amount of material so that the WD might be losing mass as a result of the TNR. However, for these simulations only 25% of the ejecta is WD material. Nevertheless, the amount of ejected material is reduced by increasing the mass accretion rate, or the initial WD luminosity, or both (Yaron et al. 2005; Starrfield et al. 2016; Hillman et al. 2015a, 2016).

Those sequences with 50% WD matter and 50% solar matter MDTNR could have either the WD losing mass ( $M_{WD} \gtrsim 1.0 M_{\odot}$ ) or gaining mass ( $M_{WD} \lesssim 1.0 M_{\odot}$ ) although only 50% of the material in the accreted layers is actual WD material. However, the peak luminosities do not agree with the observations. We assert, therefore, that for most observed CO CNe less than half of the material in the accreted region comes from the WD and it is gaining in mass as a result of accretion, TNR, and ejection.

We end this subsection with plots of the evolution of the bolometric magnitude ( $M_{bol}$ ) with time. Figure 9 shows the first hours of the evolution of both sets of simulations (top panel: 25-75 MDTNR and bottom panel: 50-50 MDTNR). Both panels show the rapid rise in  $M_{bol}$  as the energy produced in the nuclear burning region reaches the surface. Subsequently, they become roughly constant with time up to the end of the simulations.  $M_{bol}$  for the  $1.35 M_{\odot}$  simulation with 25% WD and 75% solar material is lower than those of the other massive WDs but they all appear to match observed CNe bolometric magnitudes. In contrast,  $M_{bol}$  for the 50% WD - 50% solar MDTNR simulations all lie above those reported for typical CNe but may agree with the bright outliers seen in Kasliwal et al. (2011). For example, their Table 5 (Kasliwal et al. 2011) lists one nova in M82 with an absolute magnitude (Gunn-g) of -10.7 and one in M81 with an absolute magnitude of -9.9. Since these values refer to photometry obtained with the Gunn-g filter and our values are absolute bolometric magnitudes, we do not attempt to put them on the same sequence. In addition, we end our simulations before those novae would have been discovered. Our predicted absolute visual magnitudes rise slowly and reach values close to those plotted for peak  $M_{bol}$  after a few hours when the  $T_{eff}$  has fallen below  $10^4 K$ .

#### 4.3. A Detailed Look at a TNR

In this subsection, we describe the evolution of the 25% WD -75% solar MDTNR simulation on a  $1.35 M_{\odot}$  CO WD in detail. The gross properties of the evolution are found in Table 2. We accrete a solar mixture until the temperature

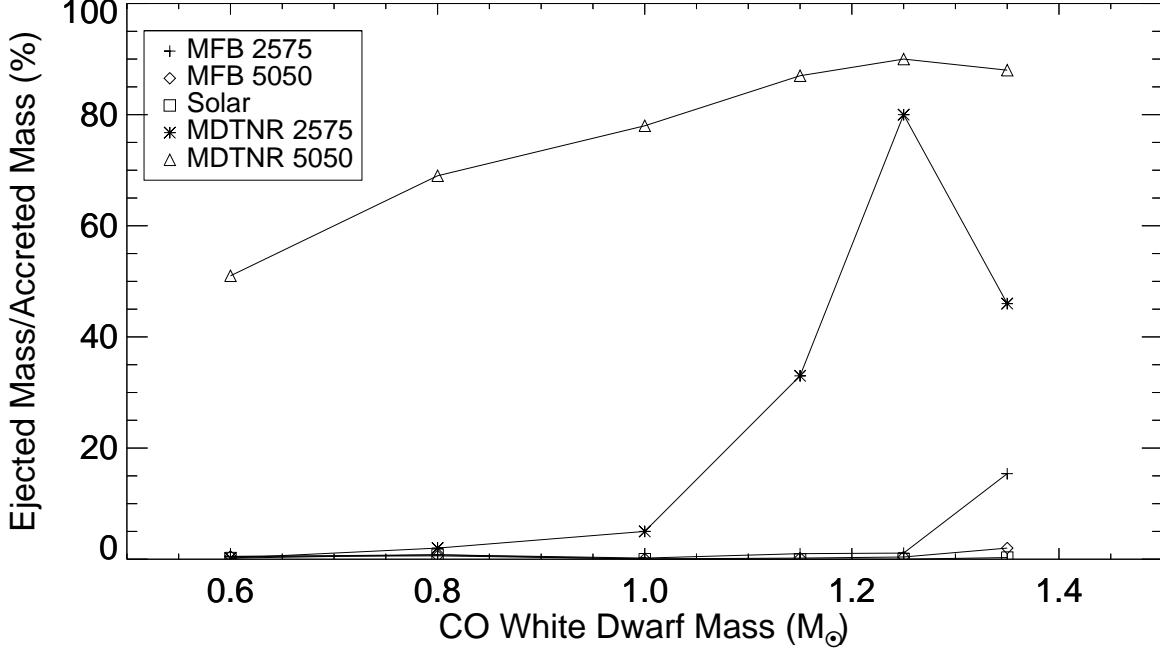


**Figure 8.** The ratio of ejected to accreted mass (in percent) as a function of CO WD mass. Neither the MFB nor the solar simulations eject much material and, thereby, the WD is growing in mass toward the Chandrasekhar Limit. While the 25% WD - 75% solar on the  $1.25M_{\odot}$  and  $1.35M_{\odot}$  simulations eject 81% and 46% of the accreted mass, respectively; only 25% of the ejecta is WD material and we predict that the WD is gaining in mass as a result of the CN outburst. The other sequences that eject a significant amount of material are the 50% WD and 50% MDTNR simulations on the massive WDs but only half of the ejecta is WD material.

has reached a value of  $7.5 \times 10^7 \text{K}$ , at which time the density is  $9.0 \times 10^3 \text{ gm cm}^{-3}$ , the pressure is  $8.8 \times 10^{19} \text{ dynes cm}^{-2}$ , and the rate of energy generation is  $6.2 \times 10^{15} \text{ erg gm}^{-1}\text{s}^{-1}$ . We then switch to the mixed composition and continue through the peak of the TNR and decline in temperature.

It takes this simulation only 0.2 s to adjust to the new composition. The convective region extends for 49 km, from the Core-Envelope Interface (CEI: the mass zone where pure WD material connects to the accreted plus WD zones), toward the surface. Because the mass of the zones decrease with increasing radius, almost 96% of the accreted layers are in the convective region so that when convection reaches the surface (about 30 s later) there is no major change in the composition. At switch-over, the mass fraction of  $^3\text{He}$  is  $2.6 \times 10^{-5}$ ,  $^2\text{H}$  is  $2.1 \times 10^{-5}$ , and  $^7\text{Be}$  is zero. We report the evolution of  $^3\text{He}$  because it is converted to  $^7\text{Be}$  through the  $^3\text{He}(\alpha, \gamma)^7\text{Be}$  reaction.  $^7\text{Be}$  then decays to  $^7\text{Li}$  with a  $\sim 53 \text{ d}$  half-life.

After 41.4 s of evolution (times are given since the beginning of the switch in composition), the sequence reaches a temperature of  $10^8 \text{K}$  just above the CEI, and after 50.4 s it reaches a peak rate of energy generation of  $3.4 \times 10^{17} \text{ erg gm}^{-1}\text{s}^{-1}$  at the CEI. The temperature in this mass zone is  $2.5 \times 10^8 \text{K}$ , the density is  $2.5 \times 10^3 \text{ gm cm}^{-3}$ , and convection has reached the surface layers of the WD. At 50.55 s (the full printout shows) the temperature has risen to  $2.7 \times 10^8 \text{K}$ , the density and nuclear energy generation have fallen to  $2.0 \times 10^3 \text{ gm cm}^{-3}$  and  $1.8 \times 10^{17} \text{ erg gm}^{-1}\text{s}^{-1}$ , respectively. At this time the mass fractions of the positron-decaying nuclei in the nuclear burning region now exceed those of most of the stable CNO nuclei ( $^{13}\text{N} = 1.7 \times 10^{-2}$ ,  $^{14}\text{O} = 1.3 \times 10^{-1}$ ,  $^{15}\text{O} = 2.6 \times 10^{-3}$ ). Any further rise in energy generation will require these nuclei to decay before being able to capture another proton (Starrfield et al. 1972; Starrfield 1989). Meanwhile, the mass fraction of  $^3\text{He}$  has fallen to  $7.6 \times 10^{-6}$  and  $^2\text{H}$  to  $4.8 \times 10^{-9}$ . The mass fraction of  $^7\text{Be}$  has risen to  $1.3 \times 10^{-5}$  at the CEI but is only  $8.7 \times 10^{-6}$  at the surface.

At an evolution time of 90.65 s (40 s after peak energy generation) the peak temperature of  $3.41 \times 10^8 \text{ K}$  is reached in the mass zones just above the CEI. The peak rate of energy generation in the same zone has declined to  $3.3 \times 10^{15} \text{ erg gm}^{-1}\text{s}^{-1}$ , and the density (in the same mass zone) to  $6.0 \times 10^2 \text{ gm cm}^{-3}$ . The temperatures throughout the nuclear burning region now exceed the Fermi temperature, lifting electron degeneracy, and the heating from the nuclear energy

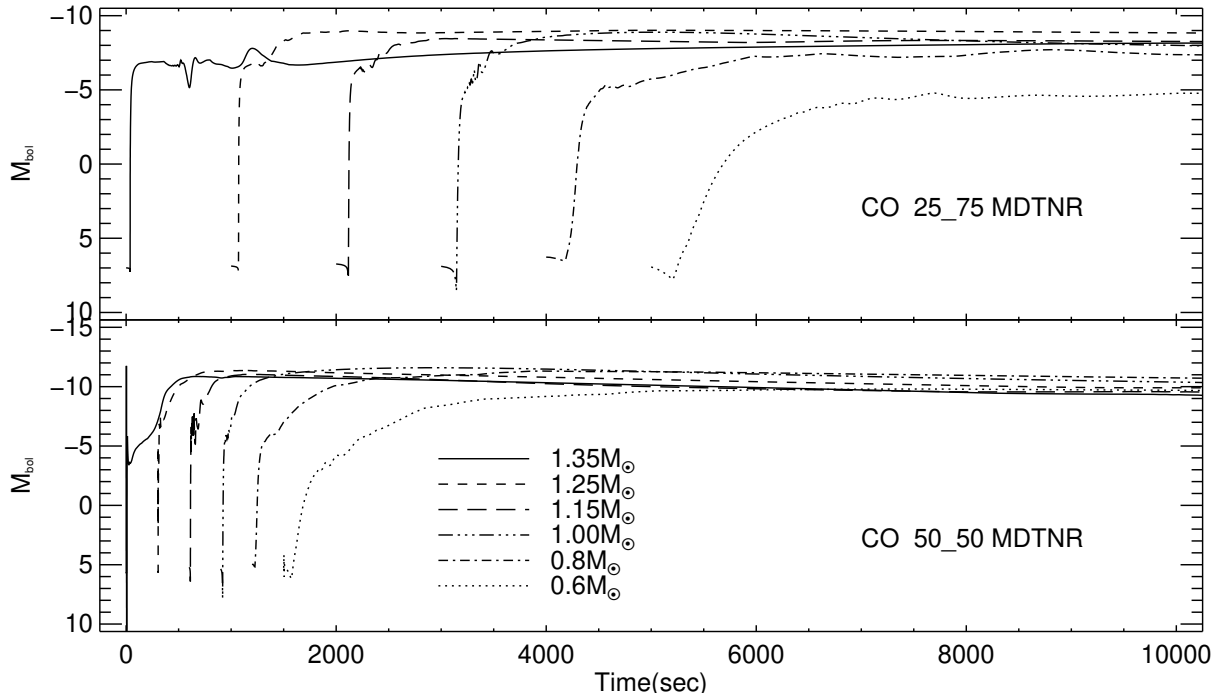


**Figure 9.** Top panel: the variation with time of the absolute bolometric magnitude for the simulations where we used a composition of 25% WD matter and 75% solar after the TNR was well underway (MDTNR). After the initial few hundred seconds they show a range in peak bolometric magnitude but there is no correlation with CO WD mass. Bottom panel: The same plot as in the top panel but for a composition of 50% WD and 50% solar. The large amount of  $^{12}\text{C}$  in these simulations drives an initial shock in the most massive WD and the other simulations all reach a peak  $M_{\text{bol}}$  around -10 which is extremely bright for the typical CN outburst. We, therefore, claim that this choice of composition does not agree with observations.

release throughout the envelope (the energy generation at the surface now exceeds  $3 \times 10^{14} \text{ erg gm}^{-1}\text{s}^{-1}$ ) has driven the luminosity to  $3.1 \times 10^4 L_{\odot}$  and  $T_{\text{eff}}$  to its peak value of  $10^6\text{K}$ .

The outer layers are expanding at  $20.8 \text{ km s}^{-1}$  and the radius of the WD has increased to 3916 km from  $\sim 2700$  km. The expansion velocity at this time is far less than the escape velocity at this radius ( $\sim 10^4 \text{ km s}^{-1}$ ). As the outer layers continue their expansion and begin to cool, convection now begins to retreat from the outer layers and thus the nuclear abundances in the material that will eventually be ejected are frozen-in. The surface abundance of  $^3\text{He}$  is  $4.4 \times 10^{-6}$ , that of  $^7\text{Be}$  is  $1.7 \times 10^{-5}$ , and  $^7\text{Li}$  is  $7.8 \times 10^{-13}$ . The destruction of the initial lithium in this type of evolution is well understood (Cameron & Fowler 1971) and implies that the  $^7\text{Li}$  and  $^7\text{Be}$  observed in nova ejecta (Tajitsu et al. 2015, 2016; Izzo et al. 2015, 2018; Molaro et al. 2016; Selvelli et al. 2018; Wagner et al. 2018) must be coming from the decay of  $^7\text{Be}$  produced in the outburst.

We continue to evolve the simulation and, after 1.1 hr of expansion, the outer layers are becoming optically thin and their velocities have reached (because of radiation pressure)  $1.4 \times 10^3 \text{ km s}^{-1}$ . The surface parameters are:  $T_{\text{eff}} = 1.3 \times 10^4\text{K}$ ,  $L = 1.3 \times 10^5 L_{\odot}$ , and the outer radius is  $5.2 \times 10^{12} \text{ cm}$ . At this distance the escape speed has declined to  $< 200 \text{ km s}^{-1}$  so that  $4.6 \times 10^{-6} M_{\odot}$  exceeds this speed, is optically thin, and we tabulate it as ejected (see Table 2). The mass fraction of  $^7\text{Be}$  is  $2.1 \times 10^{-5}$  in the ejected gases.

## 5. NUCLEOSYNTHESIS

In this section we discuss the nucleosynthesis results from our simulations. We provide these results both as tables of the ejecta abundances in mass fraction and production plots. Figure 10 (top panel:  $1.0 M_{\odot}$  25.75 MDTNR; bottom panel:  $1.35 M_{\odot}$  25.75 MDTNR) and Figure 11 (top panel:  $1.0 M_{\odot}$  50.50 MDTNR; bottom panel:  $1.35 M_{\odot}$  50.50 MDTNR) show the abundances of the stable isotopes (but also including  $^7\text{Be}$ ) divided by the Lodders (2003) solar abundances. In these two figures, the  $x$ -axis is the atomic mass number and the  $y$ -axis is the logarithmic ratio of the ejecta abundance divided by the solar abundance of the same isotope. The most abundant isotope of a given element is

marked by an asterisk and isotopes of the same element are connected by solid lines and labeled by the given element. In the next subsection, we present the  ${}^7\text{Be}$  results and then follow with a subsection on the other isotopes.

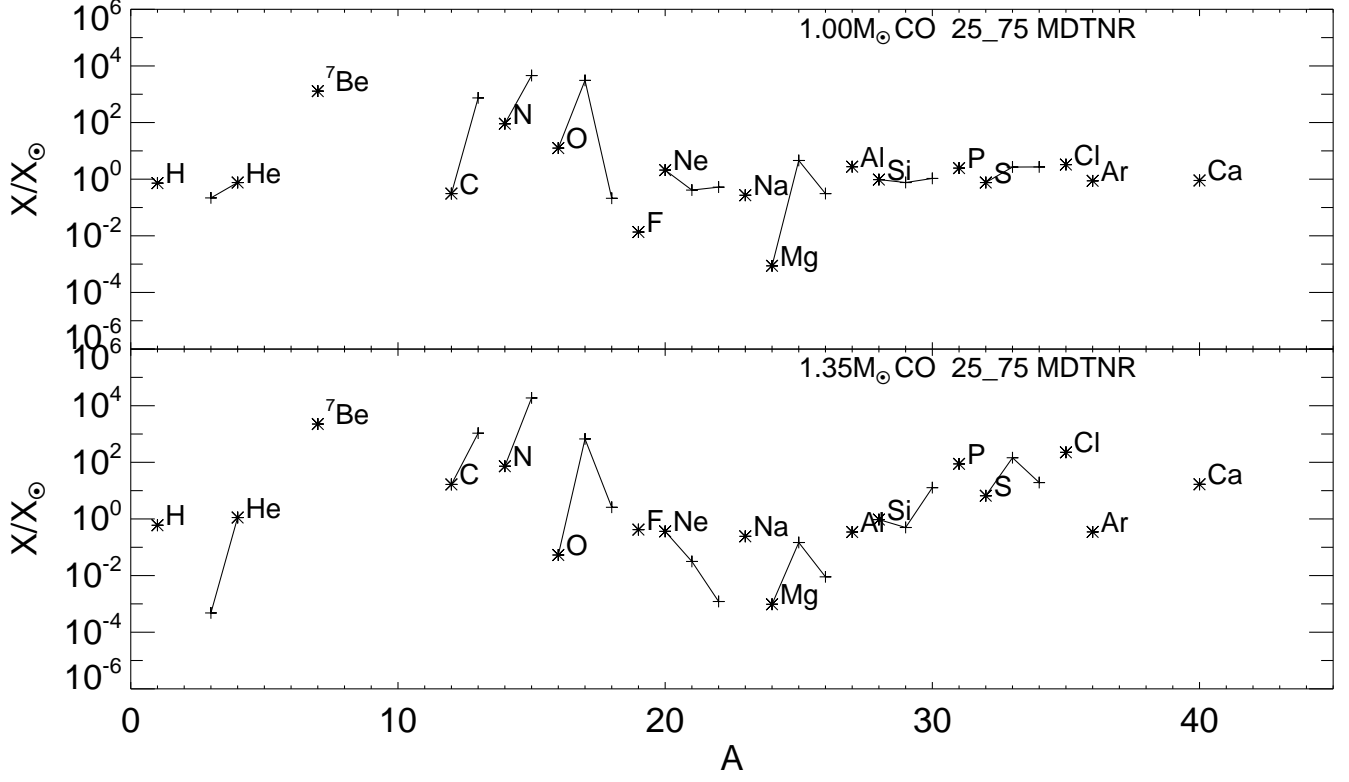


**Figure 10.** Top panel: the abundances of the stable isotopes from hydrogen to calcium in the ejecta for the  $1.0 M_{\odot}$  CO WD sequence. The  $x$ -axis is the atomic mass and the  $y$ -axis is the logarithmic ratio of the abundance divided by the solar abundance (Lodders 2003). We also include  ${}^7\text{Be}$  in this plot, even though it is radioactive, because of its large overproduction. Both the initial  ${}^7\text{Li}$  and  ${}^6\text{Li}$  are depleted during the evolution. As in Timmes et al. (1995), the most abundant isotope of a given element is designated by an “\*” and all isotopes of a given element are connected by solid lines. Any isotope above 1.0 is overproduced in the ejecta and a number of light, odd isotopes are significantly enriched in the ejecta as is  ${}^7\text{Be}$ . Bottom panel: the same plot as the top panel but for the  $1.35 M_{\odot}$  simulation with 25% WD matter and 75% solar matter. Because of the higher peak temperature in this simulation, in addition to the light, odd isotopes of carbon, nitrogen, and oxygen, phosphorus, and chlorine are also enriched.

### 5.1. The production of ${}^7\text{Be}$ in CO classical novae

Because of the recent discoveries of  ${}^7\text{Be}$ , and its decay product  ${}^7\text{Li}$ , in CNe ejecta, we report in this section that our mixed CO sequences are ejecting amounts of  ${}^7\text{Be}$  (which decays to  ${}^7\text{Li}$  after the simulation has ended) that are significantly enriched with respect to solar  ${}^7\text{Li}$ .

In Table 3 we compare the values in both our MFB and MDTNR studies with those in Hernanz et al. (1996), José & Hernanz (1998), and Rukeya et al. (2017). Rukeya et al. (2017) also provide a comparison with José & Hernanz (1998). Although there are differences between the microphysics in SHIVA (José & Hernanz 1998) and NOVA (opacities, equations of state, nuclear reaction rate library) and in the treatment of convection, except for the simulation at  $0.6 M_{\odot}$ , there is good agreement in our 2 predictions of  ${}^7\text{Li}$  ejecta abundances. The agreement is also good comparing our results with Rukeya et al. (2017) who used MESA (Paxton et al. 2011, 2013, 2015, 2016, 2018) in their study.

The top row lists the WD mass and the next row gives the specific mixture, either 25% WD matter or 50% WD matter. The next set of rows is the comparison of the  ${}^7\text{Be}$  results from each of the studies listed in the left column. The values in the first three rows all assume MFB. The results from José & Hernanz (1998) are higher than those of Rukeya et al. (2017) except for that of 25% WD matter at  $0.8 M_{\odot}$ . However, the last column, in which José &

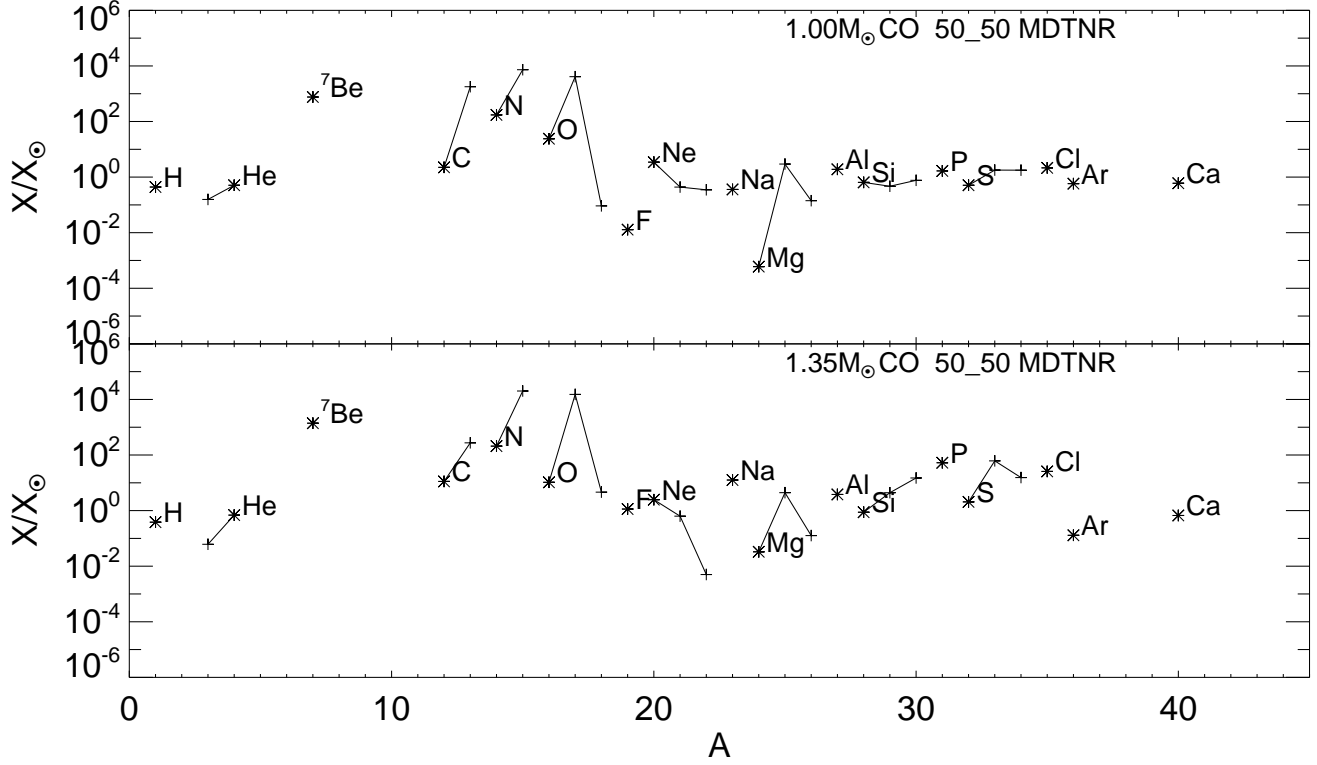


**Figure 11.** Top panel: the same plot as in Figure 10 but for the  $1.0 M_{\odot}$  simulation with 50% WD matter and 50% solar matter. The most enriched species are  $^{13}\text{C}$ ,  $^{15}\text{N}$ ,  $^{17}\text{O}$ , and  $^7\text{Be}$ . Bottom panel: the same plot as the bottom panel in Figure 10 but for the simulation with a mass of  $1.35 M_{\odot}$  and the 50% WD and 50% solar composition.

**Table 3.** Comparison of both  $^7\text{Be}$  ejecta and Ejected Mass results with José and Hernanz (1998) and Rukeya et al. (2017)

| CO WD Mass ( $M_{\odot}$ ):                              | 0.8                  | 0.8                  | 1.0                  | 1.15                 | 1.15                 | 1.15 <sup>a</sup>    |
|--|----------------------|----------------------|----------------------|----------------------|----------------------|----------------------|
| Core % <sup>b</sup>                                      | 25                   | 50                   | 50                   | 25                   | 50                   | 50                   |
| <b><math>^7\text{Be}</math> ejecta abundance by mass</b> |                      |                      |                      |                      |                      |                      |
| José & Hernanz (1998)                                    | $4.4 \times 10^{-7}$ | $9.6 \times 10^{-7}$ | $3.1 \times 10^{-6}$ | $6.0 \times 10^{-6}$ | $8.1 \times 10^{-6}$ | $3.1 \times 10^{-6}$ |
| Rukeya et al. (2017)                                     | $5.5 \times 10^{-7}$ | $4.6 \times 10^{-7}$ | $1.6 \times 10^{-6}$ | $4.3 \times 10^{-6}$ | $2.9 \times 10^{-6}$ |                      |
| MFB (This Work)  | $8.2 \times 10^{-7}$ | $7.0 \times 10^{-7}$ | $1.4 \times 10^{-6}$ | $5.9 \times 10^{-6}$ | $4.4 \times 10^{-6}$ |                      |
| MDTNR (This Work)  | $3.7 \times 10^{-6}$ | $3.5 \times 10^{-6}$ | $7.1 \times 10^{-6}$ | $1.9 \times 10^{-5}$ | $1.2 \times 10^{-5}$ |                      |
| <b>Ejected Mass (<math>M_{\odot}</math>)</b>             |                      |                      |                      |                      |                      |                      |
| José & Hernanz (1998)                                    | $7.0 \times 10^{-5}$ | $6.4 \times 10^{-5}$ | $2.3 \times 10^{-5}$ | $1.5 \times 10^{-5}$ | $1.3 \times 10^{-5}$ | $6.3 \times 10^{-6}$ |
| Rukeya et al. (2017)                                     | $2.0 \times 10^{-5}$ | $1.3 \times 10^{-5}$ | $8.2 \times 10^{-6}$ | $4.9 \times 10^{-6}$ | $3.6 \times 10^{-6}$ |                      |
| MFB (This Work)  | $3.7 \times 10^{-7}$ | $4.1 \times 10^{-7}$ | $4.4 \times 10^{-8}$ | $9.8 \times 10^{-8}$ | $1.3 \times 10^{-7}$ |                      |
| MDTNR (This Work)  | $2.9 \times 10^{-6}$ | $1.1 \times 10^{-4}$ | $6.3 \times 10^{-5}$ | $1.3 \times 10^{-5}$ | $3.4 \times 10^{-5}$ |                      |

<sup>a</sup>This sequence is reported on in Table 2 of José & Hernanz (1998) and uses the updated opacities of Iglesias & Rogers (1993)

<sup>b</sup>The numbers in this row are the percent of core material in the simulation.

Hernanz (1998) redid the same evolutionary sequence, as in the previous column, but with the Iglesias & Rogers (1993) opacities, is nearly identical to that of Rukeya et al. (2017). Comparing our MFB simulations to those above, however, we find that our  ${}^7\text{Be}$  predictions exceed those of Rukeya et al. (2017) except for the simulation with 50% core matter on a  $1.0 M_{\odot}$  WD. In contrast, they fall below those of José & Hernanz (1998) except for the simulations with 25% core matter at  $0.8 M_{\odot}$  and their last simulation with the new opacities. Nevertheless, our MDTNR results are always larger than those reported in both the other studies and our MDTNR value for 50% core matter on a  $1.15 M_{\odot}$  WD is 4 times larger than the value reported in José & Hernanz (1998) using newer opacities.

We also show in this table the comparison of the amount of ejected mass. For these cases, the sequences listed for José & Hernanz (1998) all eject more mass than either Rukeya et al. (2017) or our MFB set of calculations. Once José & Hernanz (1998) switch to an updated opacity table, however, their ejected mass drops by a factor of two and is more in line with Rukeya et al. (2017). Our MFB results are considerably smaller than either of the other two studies. In tests done to better understand this difference, we find that the introduction of new electron degenerate conductivities strongly effects the structure of the TNR and reduces the amount of ejected material. In addition, José & Hernanz (1998) use fewer mass zones ( $\sim 35$ ) with (probably) larger masses. However, comparing our MDTNR values for the amount of mass ejected, they are larger than José & Hernanz (1998) for the 3 simulations with 50% core material but smaller for the  $0.8 M_{\odot}$  (25% core matter) and the  $1.15 M_{\odot}$  (25% core matter). Finally, except for the simulation with 25% WD matter at  $0.8 M_{\odot}$ , they are all larger than the equivalent simulations by Rukeya et al. (2017).

The amount of  ${}^7\text{Li}$  (actually produced as  ${}^7\text{Be}$ ) in the ejected material in solar masses is shown in Figure 12 as a function of CO WD mass. All our MDTNR sequences eject material enriched in  ${}^7\text{Be}$  and the amount of enrichment is an increasing function of CO WD mass (Hernanz et al. 1996; José & Hernanz 1998). The nucleus produced during the TNR is  ${}^7\text{Be}$ . However, we do not follow the simulations sufficiently long for  ${}^7\text{Be}$  to decay to  ${}^7\text{Li}$ . All the initial  ${}^7\text{Li}$  (or  ${}^6\text{Li}$ ) in the accreting material is destroyed by the TNR. Both Table 1 and 2 give the  ${}^7\text{Li}$  abundance (assuming that the  ${}^7\text{Be}$  has decayed) as the amount of  ${}^7\text{Li}$  ejected with respect to the solar value ( $N({}^7\text{Li}/\text{H})_{\text{ej}}/N({}^7\text{Li}/\text{H})_{\odot}$ ).

## 5.2. Enrichment of the other Nuclei in CO novae ejecta

Figures 10 and 11 show for both WD masses and compositions that  ${}^7\text{Be}$ ,  ${}^{15}\text{N}$ ,  ${}^{17}\text{O}$ ,  ${}^{31}\text{P}$ ,  ${}^{35}\text{Cl}$ , and  ${}^{40}\text{Ca}$  are significantly overproduced in CN ejecta. The results for the  $1.0 M_{\odot}$  sequences are given in the top panels of Figures 10 and 11 and they show that both  ${}^7\text{Be}$  and  ${}^{13}\text{C}$  are about 300 times solar and  ${}^{15}\text{N}$  and  ${}^{17}\text{O}$  are nearly  $10^4$  times solar. In contrast, both  ${}^{18}\text{O}$  and  ${}^{18}\text{F}$  are depleted. None of the other isotopes are significantly enriched in the  $1.0 M_{\odot}$  sequences. The  $1.35 M_{\odot}$  results are shown in the bottom panels of Figure 10 and Figure 11. Table 2 shows that peak temperatures in the 50% WD - 50% solar sequences are much higher than in the 25% WD - 75% solar sequences. Thus,  ${}^{13}\text{C}$ ,  ${}^{15}\text{N}$ ,  ${}^{17}\text{O}$ ,  ${}^{29}\text{S}$ ,  ${}^{31}\text{P}$ , and  ${}^{35}\text{Cl}$  are a great deal more enriched in the 50% WD - 50% solar sequence. In addition,  ${}^7\text{Be}$  is enriched by about a factor of 300 and  ${}^{22}\text{Ne}$  is depleted as is  ${}^{23}\text{Na}$ .

Tables 4, 5, and 6 provide the detailed isotopic abundances in the ejected matter and allow us to compare the results for different WD masses. We do not include similar tables for the MFB simulations since they hardly ejected any material. Table 4 (no mixing of accreted with core material, hence, a solar mixture only) allows us to make predictions for those CNe or RNe that do not mix with WD matter. It shows that the ejected  ${}^{12}\text{C}$  abundance increases with WD mass, while  ${}^{14}\text{N}$  is relatively constant and the  ${}^{16}\text{O}$  abundance declines with increasing WD mass. The odd isotopes, such as  ${}^{13}\text{C}$ , increase with CO WD mass. For WD masses that exceed  $1.0 M_{\odot}$  the  ${}^{13}\text{C}$  abundance always exceeds that of  ${}^{12}\text{C}$ . The  ${}^{15}\text{N}$  abundance increases with CO WD mass and for some ranges in WD mass ( $1.0 M_{\odot}$  to  $1.25 M_{\odot}$ ) its abundance exceeds that of  ${}^{14}\text{N}$ . In contrast,  ${}^{18}\text{O}$ ,  ${}^{26}\text{Al}$ , and  ${}^{27}\text{Al}$  decrease with increasing CO WD mass. The abundance of  ${}^4\text{He}$  increases with WD mass, implying that more hydrogen is burned to helium to produce the energy radiated by the outburst, since the amount of accreted mass declines with increasing WD mass.

Table 5 gives the ejecta abundances for the mixture with 25% WD matter and 75% solar matter. The abundance of  ${}^7\text{Be}$  clearly increases with increasing WD mass and the initial  ${}^7\text{Li}$  is destroyed by the TNR. Both  ${}^{12}\text{C}$  and  ${}^{13}\text{C}$  are produced in the higher mass CO WDs but there is more  ${}^{12}\text{C}$  than  ${}^{13}\text{C}$  produced for most WD masses. The abundance of  ${}^{14}\text{N}$  is roughly constant for the more massive CO WDs while  ${}^{15}\text{N}$  reaches a peak abundance of 0.12 for a  $1.25 M_{\odot}$  WD and is nearly that value for the other massive WDs. Moreover, its abundance exceeds that of  ${}^{14}\text{N}$  for WD masses from  $1.15 M_{\odot}$  to  $1.35 M_{\odot}$ . In contrast to the solar abundance results (Table 4), the abundance of  ${}^{17}\text{O}$ ,  ${}^{18}\text{O}$ , and  ${}^{31}\text{P}$  increase with WD mass.  ${}^{26}\text{Al}$  and  ${}^{27}\text{Al}$  reach a maximum abundance at  $1.0 M_{\odot}$  and then decline with increasing WD mass as the peak temperature in the nuclear burning region increases during the TNR. The ratio of their abundances is  $\sim 0.2$ .

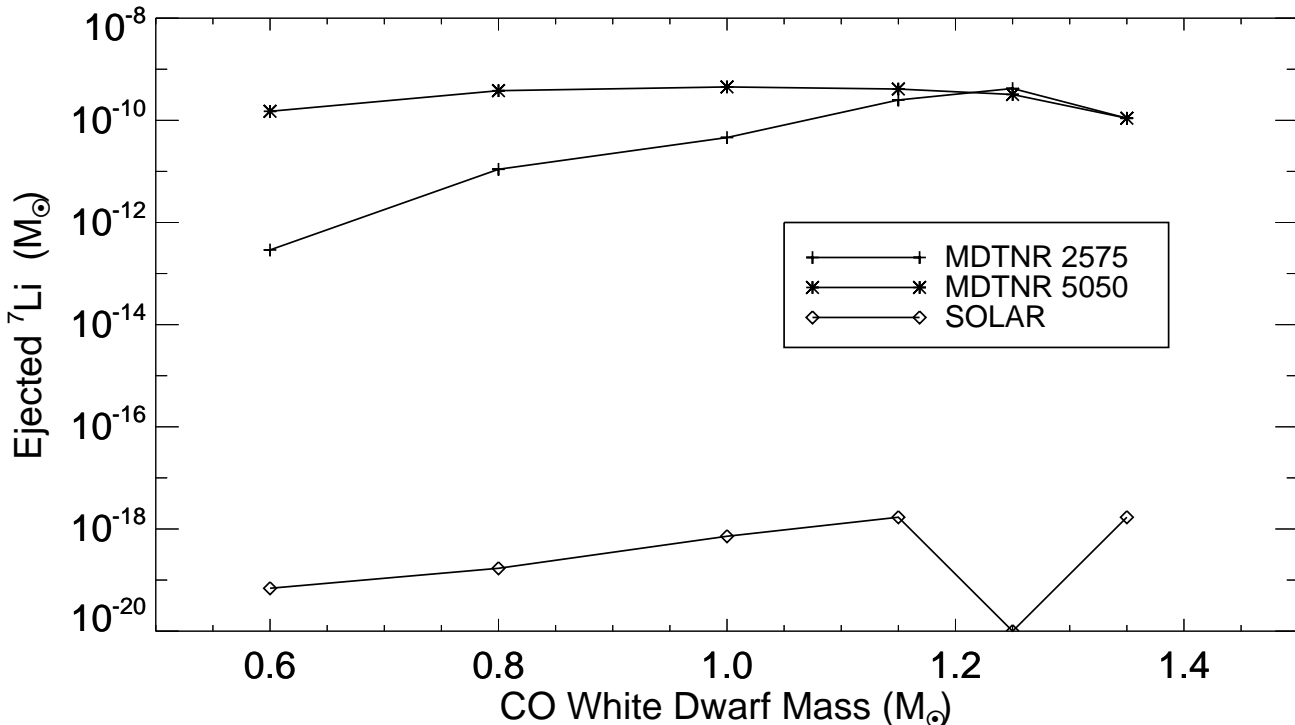


**Figure 12.** The predicted  ${}^7\text{Li}$  abundance in the ejecta as a function of WD mass in units of solar masses. The TNRs on CO WDs reach sufficiently high temperatures to deplete the initial  ${}^7\text{Li}$  present in the accreted material. The TNR then produces  ${}^7\text{Be}$  which is mixed to the surface by strong convection during the TNR and we actually plot that nucleus.  ${}^7\text{Be}$  decays ( $\sim 53$  day half-life) after the end of the simulations. The simulations where we mix from the beginning (MFB) eject far less  ${}^7\text{Li}$  and are not plotted here. The simulation with solar abundances on a  $1.25 M_{\odot}$  WD did not eject any material.

Table 6 provides a listing of the ejecta abundances for the mixture with 50% WD matter and 50% solar matter. Again, the ejected hydrogen abundance declines with increasing WD mass because the total envelope mass decreases with increasing WD mass so that it takes more hydrogen burning to provide the energy observed in the outburst. The  ${}^7\text{Be}$  abundance reaches a maximum at  $1.25 M_{\odot}$  but the  ${}^7\text{Li}$  abundance decreases with increasing WD mass.  ${}^7\text{Li}$  is essentially destroyed in the outburst so that, again, all the  ${}^7\text{Li}$  observed in CNe ejecta must be coming from the decay of  ${}^7\text{Be}$  produced in the outburst.

The ejecta abundance of  ${}^{12}\text{C}$  increases with WD mass while that of  ${}^{13}\text{C}$  is maximum at  $0.8 M_{\odot}$  and then declines. The abundance of  ${}^{14}\text{N}$  increases with WD mass while  ${}^{15}\text{N}$  increases and reaches a maximum at  $1.25 M_{\odot}$ . In fact, the odd isotopes are so abundant that molecular studies of CN ejecta should discover large amounts of  ${}^{12}\text{C}{}^{15}\text{N}$ ,  ${}^{13}\text{C}{}^{14}\text{N}$ , and in some cases  ${}^{13}\text{C}{}^{15}\text{N}$ . The detection of these molecular species would provide strong observational support for the results of these simulations, and possibly could be used to determine the composition of the underlying WD.

The abundance of  ${}^{16}\text{O}$  declines with increasing WD mass while that of  ${}^{17}\text{O}$  increases but reaches a maximum value at  $1.25 M_{\odot}$ . In contrast, that of  ${}^{18}\text{O}$  increases as the WD mass increases. The abundance of  ${}^{26}\text{Al}$  reaches a maximum at  $1.0 M_{\odot}$  while that of  ${}^{27}\text{Al}$  increases up to  $1.35 M_{\odot}$ . The ratio of their abundances varies from about 0.3 down to about 0.1, values which are smaller than found in the 25% WD - 75% solar MDTNR studies. The abundances of  ${}^{22}\text{Na}$ ,  ${}^{31}\text{P}$  and  ${}^{35}\text{Cl}$  also increase with CO WD mass.

## 6. COULD CNE AND CVS BE PROGENITORS OF SN IA?

Although of great importance to both galactic chemical evolution and, in addition, as probes of the evolution of the universe, the progenitors of SN Ia explosions are as yet unknown. Originally, the single-degenerate scenario, with the WD accreting from the secondary and growing in mass toward the Chandrasekhar Limit, was preferred but this

**Table 4.** Ejecta or Surface Abundances for Solar Accretion and No Mixing with Core Material<sup>a</sup>

| WD Mass ( $M_{\odot}$ ): | 0.6                   | 0.8                   | 1.0                   | 1.15                  | 1.25 <sup>b</sup>     | 1.35                  |
|--------------------------|-----------------------|-----------------------|-----------------------|-----------------------|-----------------------|-----------------------|
| H                        | $7.0 \times 10^{-1}$  | $7.0 \times 10^{-1}$  | $7.0 \times 10^{-1}$  | $6.7 \times 10^{-1}$  | $6.7 \times 10^{-1}$  | $6.4 \times 10^{-1}$  |
| <sup>3</sup> He          | $7.5 \times 10^{-12}$ | $3.0 \times 10^{-12}$ | $2.0 \times 10^{-7}$  | $2.0 \times 10^{-8}$  | $5.6 \times 10^{-13}$ | $8.6 \times 10^{-11}$ |
| <sup>4</sup> He          | $2.9 \times 10^{-1}$  | $3.0 \times 10^{-1}$  | $2.9 \times 10^{-1}$  | $3.1 \times 10^{-1}$  | $3.2 \times 10^{-1}$  | $3.5 \times 10^{-1}$  |
| <sup>7</sup> Be          | $1.0 \times 10^{-13}$ | $1.4 \times 10^{-13}$ | $1.5 \times 10^{-10}$ | $4.5 \times 10^{-11}$ | $4.4 \times 10^{-12}$ | $5.7 \times 10^{-11}$ |
| <sup>7</sup> Li          | 0.0                   | 0.0                   | $6.3 \times 10^{-11}$ | $6.0 \times 10^{-12}$ | 0.0                   | $7.4 \times 10^{-15}$ |
| <sup>12</sup> C          | $1.9 \times 10^{-4}$  | $3.4 \times 10^{-4}$  | $4.6 \times 10^{-4}$  | $8.8 \times 10^{-4}$  | $7.2 \times 10^{-4}$  | $1.1 \times 10^{-3}$  |
| <sup>13</sup> C          | $1.1 \times 10^{-4}$  | $3.0 \times 10^{-4}$  | $6.0 \times 10^{-4}$  | $1.5 \times 10^{-3}$  | $1.1 \times 10^{-3}$  | $2.1 \times 10^{-3}$  |
| <sup>14</sup> N          | $7.5 \times 10^{-3}$  | $7.8 \times 10^{-3}$  | $3.3 \times 10^{-3}$  | $3.4 \times 10^{-3}$  | $3.3 \times 10^{-3}$  | $3.8 \times 10^{-3}$  |
| <sup>15</sup> N          | $5.9 \times 10^{-6}$  | $4.2 \times 10^{-5}$  | $4.8 \times 10^{-3}$  | $3.6 \times 10^{-3}$  | $4.4 \times 10^{-3}$  | $2.3 \times 10^{-3}$  |
| <sup>16</sup> O          | $1.9 \times 10^{-3}$  | $1.1 \times 10^{-3}$  | $4.6 \times 10^{-4}$  | $3.0 \times 10^{-5}$  | $7.2 \times 10^{-6}$  | $1.7 \times 10^{-5}$  |
| <sup>17</sup> O          | $1.2 \times 10^{-5}$  | $7.7 \times 10^{-6}$  | $1.2 \times 10^{-4}$  | $9.4 \times 10^{-6}$  | $9.6 \times 10^{-7}$  | $6.1 \times 10^{-7}$  |
| <sup>18</sup> O          | $5.7 \times 10^{-9}$  | $3.1 \times 10^{-9}$  | $1.3 \times 10^{-7}$  | $1.8 \times 10^{-8}$  | $3.2 \times 10^{-10}$ | $8.1 \times 10^{-10}$ |
| <sup>18</sup> F          | $4.6 \times 10^{-11}$ | $1.4 \times 10^{-10}$ | $2.7 \times 10^{-9}$  | $6.9 \times 10^{-10}$ | $2.3 \times 10^{-11}$ | $5.6 \times 10^{-11}$ |
| <sup>19</sup> F          | $8.1 \times 10^{-11}$ | $1.3 \times 10^{-11}$ | $2.9 \times 10^{-9}$  | $3.1 \times 10^{-10}$ | $2.5 \times 10^{-12}$ | $6.3 \times 10^{-11}$ |
| <sup>20</sup> Ne         | $1.2 \times 10^{-3}$  | $1.2 \times 10^{-3}$  | $1.2 \times 10^{-3}$  | $7.0 \times 10^{-4}$  | $1.0 \times 10^{-4}$  | $6.0 \times 10^{-7}$  |
| <sup>21</sup> Ne         | $2.3 \times 10^{-8}$  | $4.0 \times 10^{-8}$  | $5.9 \times 10^{-7}$  | $2.6 \times 10^{-7}$  | $4.1 \times 10^{-8}$  | $3.0 \times 10^{-10}$ |
| <sup>22</sup> Ne         | $3.6 \times 10^{-5}$  | $3.8 \times 10^{-5}$  | $2.4 \times 10^{-5}$  | $7.2 \times 10^{-7}$  | $4.2 \times 10^{-11}$ | $1.6 \times 10^{-9}$  |
| <sup>22</sup> Na         | $2.3 \times 10^{-6}$  | $9.8 \times 10^{-7}$  | $1.8 \times 10^{-6}$  | $1.9 \times 10^{-6}$  | $1.4 \times 10^{-7}$  | $3.6 \times 10^{-8}$  |
| <sup>23</sup> Na         | $6.3 \times 10^{-6}$  | $3.2 \times 10^{-6}$  | $5.3 \times 10^{-6}$  | $5.7 \times 10^{-6}$  | $3.9 \times 10^{-7}$  | $1.1 \times 10^{-7}$  |
| <sup>24</sup> Mg         | $5.6 \times 10^{-8}$  | $3.2 \times 10^{-8}$  | $3.4 \times 10^{-6}$  | $3.7 \times 10^{-7}$  | $4.4 \times 10^{-9}$  | $2.8 \times 10^{-9}$  |
| <sup>25</sup> Mg         | $6.0 \times 10^{-4}$  | $3.3 \times 10^{-4}$  | $5.6 \times 10^{-5}$  | $6.3 \times 10^{-6}$  | $3.9 \times 10^{-7}$  | $3.7 \times 10^{-8}$  |
| <sup>26</sup> Mg         | $7.7 \times 10^{-5}$  | $2.4 \times 10^{-5}$  | $5.3 \times 10^{-6}$  | $4.3 \times 10^{-7}$  | $1.6 \times 10^{-8}$  | $2.4 \times 10^{-9}$  |
| <sup>26</sup> Al         | $2.9 \times 10^{-5}$  | $2.0 \times 10^{-5}$  | $6.5 \times 10^{-6}$  | $8.5 \times 10^{-7}$  | $1.0 \times 10^{-7}$  | $1.6 \times 10^{-9}$  |
| <sup>27</sup> Al         | $9.7 \times 10^{-5}$  | $1.4 \times 10^{-4}$  | $3.0 \times 10^{-5}$  | $4.3 \times 10^{-6}$  | $4.3 \times 10^{-7}$  | $1.9 \times 10^{-8}$  |
| <sup>28</sup> Si         | $7.8 \times 10^{-4}$  | $1.1 \times 10^{-3}$  | $1.6 \times 10^{-3}$  | $7.3 \times 10^{-4}$  | $6.6 \times 10^{-5}$  | $5.2 \times 10^{-7}$  |
| <sup>29</sup> Si         | $4.0 \times 10^{-5}$  | $3.6 \times 10^{-5}$  | $2.2 \times 10^{-5}$  | $1.3 \times 10^{-5}$  | $9.1 \times 10^{-7}$  | $6.0 \times 10^{-8}$  |
| <sup>30</sup> Si         | $2.7 \times 10^{-5}$  | $3.1 \times 10^{-5}$  | $8.8 \times 10^{-5}$  | $6.5 \times 10^{-4}$  | $6.5 \times 10^{-5}$  | $3.1 \times 10^{-7}$  |
| <sup>31</sup> P          | $7.5 \times 10^{-6}$  | $7.2 \times 10^{-6}$  | $9.9 \times 10^{-6}$  | $8.7 \times 10^{-5}$  | $8.2 \times 10^{-6}$  | $1.2 \times 10^{-7}$  |
| <sup>32</sup> S          | $4.0 \times 10^{-4}$  | $4.0 \times 10^{-4}$  | $4.0 \times 10^{-4}$  | $1.7 \times 10^{-3}$  | $3.9 \times 10^{-3}$  | $6.4 \times 10^{-4}$  |
| <sup>33</sup> S          | $3.2 \times 10^{-6}$  | $3.2 \times 10^{-6}$  | $2.9 \times 10^{-6}$  | $2.3 \times 10^{-6}$  | $8.0 \times 10^{-6}$  | $2.2 \times 10^{-6}$  |
| <sup>34</sup> S          | $1.9 \times 10^{-5}$  | $1.8 \times 10^{-5}$  | $1.6 \times 10^{-5}$  | $2.5 \times 10^{-6}$  | $6.7 \times 10^{-6}$  | $2.4 \times 10^{-6}$  |
| <sup>35</sup> Cl         | $4.1 \times 10^{-6}$  | $4.4 \times 10^{-6}$  | $6.9 \times 10^{-6}$  | $1.7 \times 10^{-5}$  | $5.9 \times 10^{-5}$  | $4.8 \times 10^{-5}$  |
| <sup>36</sup> Ar         | $9.1 \times 10^{-5}$  | $9.1 \times 10^{-5}$  | $7.8 \times 10^{-5}$  | $5.1 \times 10^{-6}$  | $5.0 \times 10^{-6}$  | $4.2 \times 10^{-6}$  |
| <sup>40</sup> Ca         | $7.1 \times 10^{-5}$  | $7.1 \times 10^{-5}$  | $7.1 \times 10^{-5}$  | $7.2 \times 10^{-5}$  | $9.4 \times 10^{-5}$  | $3.6 \times 10^{-3}$  |

<sup>a</sup>All abundances are Mass Fraction<sup>b</sup>These are the surface zone abundances since no material was ejected.

scenario is now disfavored by many (Gilfanov & Bogdán 2010, and references therein). The other scenario, the double-degenerate scenario, which involves either a merger or collision between two CO WDs, is now thought to be the major channel for SN Ia explosions. The cause of this switch in the preferred explosion paradigm is a number of perceived problems with the single-degenerate scenario that need to be understood. In this section we discuss four of those problems and show that they are, in fact, not problems at all.

The first major problem, which is directly relevant to the simulations presented in the earlier sections, is the common assumption, based on the analyses of the ejecta abundances and ejecta masses of CNe outbursts that the WD

**Table 5.** Ejecta Abundances for 25-75 MDTNR mixture in CO White Dwarfs<sup>a</sup>

| WD Mass ( $M_{\odot}$ ) | 0.6                   | 0.8                   | 1.0                   | 1.15                  | 1.25                  | 1.35                  |
|-------------------------|-----------------------|-----------------------|-----------------------|-----------------------|-----------------------|-----------------------|
| H                       | $5.3 \times 10^{-1}$  | $5.2 \times 10^{-1}$  | $5.1 \times 10^{-1}$  | $4.8 \times 10^{-1}$  | $4.6 \times 10^{-1}$  | $4.3 \times 10^{-1}$  |
| <sup>3</sup> He         | $3.5 \times 10^{-5}$  | $1.6 \times 10^{-5}$  | $6.4 \times 10^{-6}$  | $4.2 \times 10^{-7}$  | $4.4 \times 10^{-8}$  | $1.4 \times 10^{-8}$  |
| <sup>4</sup> He         | $2.1 \times 10^{-1}$  | $2.1 \times 10^{-1}$  | $2.1 \times 10^{-1}$  | $2.3 \times 10^{-1}$  | $2.7 \times 10^{-1}$  | $3.1 \times 10^{-1}$  |
| <sup>7</sup> Be         | $6.0 \times 10^{-7}$  | $3.7 \times 10^{-6}$  | $1.2 \times 10^{-5}$  | $1.9 \times 10^{-5}$  | $2.0 \times 10^{-5}$  | $2.1 \times 10^{-5}$  |
| <sup>7</sup> Li         | $4.8 \times 10^{-10}$ | $7.1 \times 10^{-13}$ | $4.0 \times 10^{-12}$ | $4.4 \times 10^{-13}$ | $3.1 \times 10^{-13}$ | $4.6 \times 10^{-13}$ |
| <sup>12</sup> C         | $9.0 \times 10^{-2}$  | $1.7 \times 10^{-2}$  | $9.3 \times 10^{-4}$  | $1.0 \times 10^{-2}$  | $2.5 \times 10^{-2}$  | $5.0 \times 10^{-2}$  |
| <sup>13</sup> C         | $3.5 \times 10^{-2}$  | $8.2 \times 10^{-2}$  | $2.5 \times 10^{-2}$  | $1.2 \times 10^{-2}$  | $2.1 \times 10^{-2}$  | $3.8 \times 10^{-2}$  |
| <sup>14</sup> N         | $5.2 \times 10^{-3}$  | $3.8 \times 10^{-2}$  | $1.0 \times 10^{-1}$  | $8.0 \times 10^{-2}$  | $7.9 \times 10^{-2}$  | $8.0 \times 10^{-2}$  |
| <sup>15</sup> N         | $2.2 \times 10^{-5}$  | $2.1 \times 10^{-3}$  | $2.1 \times 10^{-2}$  | $9.7 \times 10^{-2}$  | $1.2 \times 10^{-1}$  | $8.4 \times 10^{-2}$  |
| <sup>16</sup> O         | $1.3 \times 10^{-1}$  | $1.3 \times 10^{-1}$  | $1.2 \times 10^{-1}$  | $4.1 \times 10^{-2}$  | $1.4 \times 10^{-3}$  | $5.4 \times 10^{-4}$  |
| <sup>17</sup> O         | $2.4 \times 10^{-4}$  | $2.0 \times 10^{-3}$  | $1.3 \times 10^{-2}$  | $3.5 \times 10^{-2}$  | $1.6 \times 10^{-2}$  | $3.3 \times 10^{-3}$  |
| <sup>18</sup> O         | $7.3 \times 10^{-7}$  | $1.8 \times 10^{-7}$  | $5.3 \times 10^{-6}$  | $1.7 \times 10^{-5}$  | $3.4 \times 10^{-5}$  | $6.7 \times 10^{-5}$  |
| <sup>18</sup> F         | $1.9 \times 10^{-9}$  | $1.0 \times 10^{-8}$  | $6.2 \times 10^{-7}$  | $1.6 \times 10^{-6}$  | $2.5 \times 10^{-6}$  | $4.3 \times 10^{-6}$  |
| <sup>19</sup> F         | $3.2 \times 10^{-7}$  | $7.4 \times 10^{-9}$  | $6.0 \times 10^{-9}$  | $8.6 \times 10^{-8}$  | $3.0 \times 10^{-7}$  | $1.9 \times 10^{-7}$  |
| <sup>20</sup> Ne        | $8.8 \times 10^{-4}$  | $8.8 \times 10^{-4}$  | $9.3 \times 10^{-4}$  | $1.5 \times 10^{-3}$  | $1.6 \times 10^{-3}$  | $4.7 \times 10^{-4}$  |
| <sup>21</sup> Ne        | $5.3 \times 10^{-7}$  | $2.3 \times 10^{-7}$  | $4.7 \times 10^{-7}$  | $6.3 \times 10^{-7}$  | $5.8 \times 10^{-7}$  | $1.1 \times 10^{-7}$  |
| <sup>22</sup> Ne        | $2.6 \times 10^{-3}$  | $2.6 \times 10^{-3}$  | $2.5 \times 10^{-3}$  | $1.4 \times 10^{-3}$  | $2.6 \times 10^{-5}$  | $5.8 \times 10^{-6}$  |
| <sup>22</sup> Na        | $1.8 \times 10^{-6}$  | $8.6 \times 10^{-7}$  | $1.4 \times 10^{-6}$  | $2.3 \times 10^{-6}$  | $5.3 \times 10^{-6}$  | $4.4 \times 10^{-6}$  |
| <sup>23</sup> Na        | $2.9 \times 10^{-5}$  | $2.6 \times 10^{-5}$  | $8.8 \times 10^{-6}$  | $1.2 \times 10^{-5}$  | $2.3 \times 10^{-5}$  | $5.9 \times 10^{-6}$  |
| <sup>24</sup> Mg        | $4.1 \times 10^{-4}$  | $4.7 \times 10^{-5}$  | $7.2 \times 10^{-7}$  | $3.3 \times 10^{-7}$  | $3.4 \times 10^{-7}$  | $3.4 \times 10^{-7}$  |
| <sup>25</sup> Mg        | $6.9 \times 10^{-5}$  | $4.5 \times 10^{-4}$  | $3.2 \times 10^{-4}$  | $7.1 \times 10^{-5}$  | $3.4 \times 10^{-5}$  | $1.2 \times 10^{-5}$  |
| <sup>26</sup> Mg        | $6.4 \times 10^{-5}$  | $6.2 \times 10^{-5}$  | $2.4 \times 10^{-5}$  | $3.0 \times 10^{-6}$  | $1.7 \times 10^{-6}$  | $1.2 \times 10^{-6}$  |
| <sup>26</sup> Al        | $1.6 \times 10^{-8}$  | $3.2 \times 10^{-6}$  | $8.4 \times 10^{-5}$  | $2.2 \times 10^{-5}$  | $8.5 \times 10^{-6}$  | $2.4 \times 10^{-6}$  |
| <sup>27</sup> Al        | $5.0 \times 10^{-5}$  | $5.1 \times 10^{-5}$  | $1.7 \times 10^{-4}$  | $1.2 \times 10^{-4}$  | $4.2 \times 10^{-5}$  | $1.5 \times 10^{-5}$  |
| <sup>28</sup> Si        | $5.7 \times 10^{-4}$  | $5.7 \times 10^{-4}$  | $6.3 \times 10^{-4}$  | $1.6 \times 10^{-3}$  | $9.1 \times 10^{-4}$  | $4.8 \times 10^{-4}$  |
| <sup>29</sup> Si        | $3.0 \times 10^{-5}$  | $3.0 \times 10^{-5}$  | $2.6 \times 10^{-5}$  | $3.0 \times 10^{-5}$  | $3.5 \times 10^{-5}$  | $1.7 \times 10^{-5}$  |
| <sup>30</sup> Si        | $2.0 \times 10^{-5}$  | $2.0 \times 10^{-5}$  | $2.5 \times 10^{-5}$  | $1.3 \times 10^{-4}$  | $5.2 \times 10^{-4}$  | $2.3 \times 10^{-4}$  |
| <sup>31</sup> P         | $5.7 \times 10^{-6}$  | $5.7 \times 10^{-6}$  | $5.7 \times 10^{-6}$  | $2.4 \times 10^{-5}$  | $2.9 \times 10^{-4}$  | $1.5 \times 10^{-4}$  |
| <sup>32</sup> S         | $3.0 \times 10^{-4}$  | $3.0 \times 10^{-4}$  | $3.0 \times 10^{-4}$  | $3.0 \times 10^{-4}$  | $2.2 \times 10^{-3}$  | $2.7 \times 10^{-3}$  |
| <sup>33</sup> S         | $2.4 \times 10^{-6}$  | $2.4 \times 10^{-6}$  | $2.4 \times 10^{-6}$  | $2.2 \times 10^{-6}$  | $1.7 \times 10^{-5}$  | $1.6 \times 10^{-4}$  |
| <sup>34</sup> S         | $1.4 \times 10^{-5}$  | $1.4 \times 10^{-5}$  | $1.4 \times 10^{-5}$  | $1.1 \times 10^{-5}$  | $7.7 \times 10^{-6}$  | $1.2 \times 10^{-4}$  |
| <sup>35</sup> Cl        | $3.0 \times 10^{-6}$  | $3.0 \times 10^{-6}$  | $3.2 \times 10^{-6}$  | $5.9 \times 10^{-6}$  | $1.4 \times 10^{-5}$  | $2.7 \times 10^{-4}$  |
| <sup>36</sup> Ar        | $6.8 \times 10^{-5}$  | $6.8 \times 10^{-5}$  | $6.8 \times 10^{-5}$  | $4.7 \times 10^{-5}$  | $3.0 \times 10^{-6}$  | $3.2 \times 10^{-5}$  |
| <sup>40</sup> Ca        | $5.4 \times 10^{-5}$  | $1.0 \times 10^{-3}$  |

<sup>a</sup>All abundances are Mass Fraction

is decreasing in mass as a consequence of the TNR and resulting explosion. As we have now shown in earlier sections, however, that assumption is incorrect and, in fact, the WD in a *CO nova outburst* is gaining in mass.

We have also shown in previous studies, in addition, that the WD is growing in mass when there is no mixing of the accreting material with WD core matter as may be occurring in CVs in general (Starrfield 2014, 2017, and references therein). These latter results are based on studies with both NOVA and MESA and imply that the consequence of mass transfer in CVs is the increasing mass of the WD. Moreover, the calculations of Hillman et al. (2015a, 2016) show that high mass accretion rates also result in the WDs growing in mass. One concern, nevertheless, is that the large number of CVs in the galaxy may result in too many SN Ia explosions. We note, however, that the mass of the secondary also determines the ultimate consequences of the evolution. It is possible that in many CV systems the

**Table 6.** Ejecta Abundances for 50-50 MDTNR mixture in CO White Dwarfs<sup>a</sup>

| WD Mass ( $M_{\odot}$ ): | 0.6                   | 0.8                   | 1.0                   | 1.15                  | 1.25                  | 1.35                  |
|--------------------------|-----------------------|-----------------------|-----------------------|-----------------------|-----------------------|-----------------------|
| H                        | $3.4 \times 10^{-1}$  | $3.3 \times 10^{-1}$  | $3.1 \times 10^{-1}$  | $3.0 \times 10^{-1}$  | $2.7 \times 10^{-1}$  | $2.2 \times 10^{-1}$  |
| <sup>3</sup> He          | $1.1 \times 10^{-5}$  | $7.6 \times 10^{-6}$  | $4.6 \times 10^{-6}$  | $1.6 \times 10^{-6}$  | $9.3 \times 10^{-7}$  | $4.4 \times 10^{-7}$  |
| <sup>4</sup> He          | $1.4 \times 10^{-1}$  | $1.4 \times 10^{-1}$  | $1.4 \times 10^{-1}$  | $1.6 \times 10^{-1}$  | $1.9 \times 10^{-1}$  | $2.4 \times 10^{-1}$  |
| <sup>7</sup> Be          | $9.3 \times 10^{-7}$  | $3.5 \times 10^{-6}$  | $7.1 \times 10^{-6}$  | $1.2 \times 10^{-5}$  | $1.4 \times 10^{-5}$  | $1.6 \times 10^{-5}$  |
| <sup>7</sup> Li          | $4.3 \times 10^{-13}$ | $2.1 \times 10^{-13}$ | $1.2 \times 10^{-13}$ | $1.2 \times 10^{-13}$ | $3.0 \times 10^{-13}$ | $7.2 \times 10^{-14}$ |
| <sup>12</sup> C          | $1.0 \times 10^{-1}$  | $2.3 \times 10^{-2}$  | $6.6 \times 10^{-3}$  | $1.7 \times 10^{-2}$  | $2.0 \times 10^{-2}$  | $3.6 \times 10^{-2}$  |
| <sup>13</sup> C          | $1.3 \times 10^{-1}$  | $1.5 \times 10^{-1}$  | $6.5 \times 10^{-2}$  | $1.2 \times 10^{-2}$  | $2.1 \times 10^{-2}$  | $1.0 \times 10^{-2}$  |
| <sup>14</sup> N          | $3.0 \times 10^{-2}$  | $9.6 \times 10^{-2}$  | $1.9 \times 10^{-1}$  | $2.0 \times 10^{-1}$  | $1.9 \times 10^{-1}$  | $1.7 \times 10^{-1}$  |
| <sup>15</sup> N          | $2.2 \times 10^{-4}$  | $5.3 \times 10^{-3}$  | $3.2 \times 10^{-2}$  | $8.8 \times 10^{-2}$  | $1.7 \times 10^{-1}$  | $2.0 \times 10^{-1}$  |
| <sup>16</sup> O          | $2.5 \times 10^{-1}$  | $2.4 \times 10^{-1}$  | $2.3 \times 10^{-1}$  | $1.8 \times 10^{-1}$  | $4.9 \times 10^{-2}$  | $1.9 \times 10^{-2}$  |
| <sup>17</sup> O          | $1.4 \times 10^{-3}$  | $4.9 \times 10^{-3}$  | $1.6 \times 10^{-2}$  | $4.3 \times 10^{-2}$  | $8.6 \times 10^{-2}$  | $3.2 \times 10^{-2}$  |
| <sup>18</sup> O          | $3.9 \times 10^{-7}$  | $8.2 \times 10^{-7}$  | $2.0 \times 10^{-6}$  | $8.3 \times 10^{-6}$  | $3.0 \times 10^{-5}$  | $6.0 \times 10^{-6}$  |
| <sup>18</sup> F          | $2.1 \times 10^{-8}$  | $4.3 \times 10^{-8}$  | $5.0 \times 10^{-7}$  | $4.0 \times 10^{-6}$  | $9.4 \times 10^{-6}$  | $1.9 \times 10^{-6}$  |
| <sup>19</sup> F          | $2.6 \times 10^{-8}$  | $8.6 \times 10^{-10}$ | $5.2 \times 10^{-9}$  | $4.2 \times 10^{-8}$  | $7.3 \times 10^{-7}$  | $1.0 \times 10^{-6}$  |
| <sup>20</sup> Ne         | $5.8 \times 10^{-4}$  | $6.0 \times 10^{-4}$  | $6.7 \times 10^{-4}$  | $1.1 \times 10^{-3}$  | $2.6 \times 10^{-3}$  | $1.3 \times 10^{-3}$  |
| <sup>21</sup> Ne         | $3.2 \times 10^{-8}$  | $1.1 \times 10^{-7}$  | $2.2 \times 10^{-7}$  | $3.8 \times 10^{-7}$  | $1.1 \times 10^{-6}$  | $4.0 \times 10^{-7}$  |
| <sup>22</sup> Ne         | $5.0 \times 10^{-3}$  | $5.0 \times 10^{-3}$  | $4.9 \times 10^{-3}$  | $4.0 \times 10^{-3}$  | $4.2 \times 10^{-4}$  | $1.9 \times 10^{-4}$  |
| <sup>22</sup> Na         | $1.2 \times 10^{-6}$  | $2.9 \times 10^{-7}$  | $4.1 \times 10^{-7}$  | $1.1 \times 10^{-6}$  | $5.1 \times 10^{-6}$  | $1.2 \times 10^{-6}$  |
| <sup>23</sup> Na         | $2.2 \times 10^{-5}$  | $2.1 \times 10^{-5}$  | $1.3 \times 10^{-5}$  | $1.3 \times 10^{-5}$  | $4.1 \times 10^{-5}$  | $2.2 \times 10^{-5}$  |
| <sup>24</sup> Mg         | $1.3 \times 10^{-4}$  | $1.1 \times 10^{-6}$  | $6.4 \times 10^{-7}$  | $7.1 \times 10^{-7}$  | $1.4 \times 10^{-6}$  | $2.4 \times 10^{-6}$  |
| <sup>25</sup> Mg         | $2.0 \times 10^{-4}$  | $3.2 \times 10^{-4}$  | $2.4 \times 10^{-4}$  | $1.8 \times 10^{-4}$  | $2.3 \times 10^{-4}$  | $8.4 \times 10^{-5}$  |
| <sup>26</sup> Mg         | $4.2 \times 10^{-5}$  | $3.7 \times 10^{-5}$  | $1.2 \times 10^{-5}$  | $9.1 \times 10^{-6}$  | $2.0 \times 10^{-5}$  | $6.8 \times 10^{-6}$  |
| <sup>26</sup> Al         | $1.8 \times 10^{-7}$  | $1.2 \times 10^{-5}$  | $6.6 \times 10^{-5}$  | $7.7 \times 10^{-5}$  | $2.9 \times 10^{-5}$  | $2.8 \times 10^{-5}$  |
| <sup>27</sup> Al         | $3.3 \times 10^{-5}$  | $3.9 \times 10^{-5}$  | $1.2 \times 10^{-4}$  | $3.0 \times 10^{-4}$  | $1.4 \times 10^{-4}$  | $1.3 \times 10^{-4}$  |
| <sup>28</sup> Si         | $3.8 \times 10^{-4}$  | $3.8 \times 10^{-4}$  | $4.2 \times 10^{-4}$  | $7.7 \times 10^{-4}$  | $2.1 \times 10^{-3}$  | $9.9 \times 10^{-4}$  |
| <sup>29</sup> Si         | $2.0 \times 10^{-5}$  | $2.0 \times 10^{-5}$  | $1.6 \times 10^{-5}$  | $1.3 \times 10^{-5}$  | $9.2 \times 10^{-5}$  | $3.3 \times 10^{-5}$  |
| <sup>30</sup> Si         | $1.4 \times 10^{-5}$  | $1.4 \times 10^{-5}$  | $1.8 \times 10^{-5}$  | $4.0 \times 10^{-5}$  | $7.9 \times 10^{-4}$  | $4.6 \times 10^{-4}$  |
| <sup>31</sup> P          | $3.8 \times 10^{-6}$  | $3.8 \times 10^{-6}$  | $3.8 \times 10^{-6}$  | $5.5 \times 10^{-6}$  | $3.0 \times 10^{-4}$  | $2.9 \times 10^{-4}$  |
| <sup>32</sup> S          | $2.0 \times 10^{-4}$  | $2.0 \times 10^{-4}$  | $2.0 \times 10^{-4}$  | $2.0 \times 10^{-4}$  | $4.9 \times 10^{-4}$  | $3.4 \times 10^{-3}$  |
| <sup>33</sup> S          | $1.6 \times 10^{-6}$  | $1.6 \times 10^{-6}$  | $1.6 \times 10^{-6}$  | $1.6 \times 10^{-6}$  | $4.0 \times 10^{-6}$  | $2.4 \times 10^{-4}$  |
| <sup>34</sup> S          | $9.3 \times 10^{-6}$  | $9.3 \times 10^{-6}$  | $9.2 \times 10^{-6}$  | $8.7 \times 10^{-6}$  | $4.4 \times 10^{-6}$  | $1.4 \times 10^{-4}$  |
| <sup>35</sup> Cl         | $2.0 \times 10^{-6}$  | $2.0 \times 10^{-6}$  | $2.1 \times 10^{-6}$  | $2.7 \times 10^{-6}$  | $6.8 \times 10^{-6}$  | $2.5 \times 10^{-4}$  |
| <sup>36</sup> Ar         | $4.6 \times 10^{-5}$  | $4.6 \times 10^{-5}$  | $4.5 \times 10^{-5}$  | $4.0 \times 10^{-5}$  | $1.1 \times 10^{-5}$  | $4.8 \times 10^{-5}$  |
| <sup>40</sup> Ca         | $3.6 \times 10^{-5}$  | $5.9 \times 10^{-5}$  |

<sup>a</sup>All abundances are Mass Fraction

secondary has too little mass and, therefore, the evolution will end before the WD has reached the Chandrasekhar Limit.

The second perceived problem is due to the *interpretation* of the calculations of Nomoto (1982) and Fujimoto (1982a,b). A reproduction of their results can be found as Figure 5 in Kahabka & van den Heuvel (1997). The figure shows that the space describing the consequences of mass accretion rate as a function of the mass of the accreting WD can be divided into three regions. For the lowest mass accretion rates, at all WD masses, it is predicted that accretion results in hydrogen flashes that resemble those of CNe and, as already discussed, the WD is thought to be losing mass. However, the purpose of this paper has been to provide a broad range of simulations at low  $\dot{M}$  that show a WD accreting at low rates is gaining in mass. Hillman et al. (2015a, 2016) have investigated the consequences of

accretion at higher rates and also find that the WD is growing in mass. Thus, mass accreting systems with a broad range in WD mass and  $\dot{M}$  must be included in the classes of SN Ia progenitors.

A third problem relates to the upper region on the [Nomoto \(1982\)](#) and the [Fujimoto \(1982a,b\)](#) plot, which shows the results for the highest accretion rates and predicts for all WD masses that the radius of the WD will grow rapidly to red giant dimensions, accretion will be halted, and any further evolution will await the collapse of the extended layers. These systems, therefore, cannot be SN Ia progenitors. However, we have done extensive studies of solar accretion onto WDs using both NOVA and MESA and our version of their diagram can be found in [Starrfield \(2014, 2017\)](#). Our fully hydrodynamic studies show, for the highest mass accretion rates on the most massive WDs, steady hydrogen burning (see below) is occurring followed by recurring helium flashes. The helium flashes do not result in ejection and the WDs are again growing in mass. [Hillman et al. \(2015a, 2016\)](#) also report that helium flashes do not eject material.

The fourth problem is based on the existence of the intermediate regime identified by [Nomoto \(1982\)](#) and [Fujimoto \(1982a,b\)](#), where the material is predicted to burn steadily at the rate it is accreted. The central  $\dot{M}$  of this region is nominally  $\sim 3 \times 10^{-7} M_{\odot} \text{ yr}^{-1}$  and it does have a slight variation with WD mass. Those systems that are accreting at the steady nuclear burning rate are supposedly evolving horizontally in this plot towards higher WD mass and, by some *unknown* mechanism, the mass transfer in the binary system is stuck in this mass accretion range. [van den Heuvel et al. \(1992\)](#) predicted that it was only the systems in this region that were SN Ia progenitors via the SD scenario, They identified the Super Soft X-ray sources (SSS) as those systems, based on their luminosities and effective temperatures. The SSS are *luminous*, massive, WDs discovered by ROSAT ([Trümper et al. 1991](#)). They are binaries, with luminosities  $L_* \sim 10^{37-38} \text{ erg s}^{-1}$  and effective temperatures ranging from  $3 - 7 \times 10^5 \text{ K}$  ([Cowley et al. 1998](#)). See also [Branch et al. \(1995\)](#) and [Kahabka & van den Heuvel \(1997\)](#).

However, in more recent studies of accretion without mixing, an expanded study of the stability of thin shells can be found in [Yoon et al. \(2004, and references therein\)](#), who investigated the accretion of helium-rich and hydrogen-rich material onto WDs. Using their results, we find that sequences in the steady nuclear burning regime begin in their stable region, but with continued accretion, evolve into instability. In addition, their study shows that the evolutionary sequences at these  $\dot{M}$  exhibit the [Schwarzschild & Härm \(1965\)](#) thin shell instability, which implies that steady burning does not occur. We identify these systems, therefore, with those CVs (dwarf, recurrent, symbiotic novae) that show no core material either on the surface of the WD or in their ejecta.

Given that the SSS were the only systems that were predicted to be single-degenerate Ia progenitors, it was expected that they would be detected by consequences of the long periods of luminous X-ray and UV emission on the surrounding ISM. In addition, this extreme emission should still be evident in the ISM surrounding recent SN Ia explosions. As an example, we quote from [Graur & Woods \(2019\)](#) "For the WD to efficiently grow in mass, the accreted hydrogen must undergo stable nuclear-burning on its surface. This means the progenitor system will be a luminous source of soft X-ray emission (a supersoft X-ray source, SSS, [van den Heuvel et al. 1992](#)) for at least some period of time before the explosion." Similar statements can also be found in [Gilfanov & Bogdán \(2010\)](#) and [Kuuttila et al. \(2019\)](#). Such emission has not been found and the absence of evidence has been used to eliminate the single degenerate scenario even in the most recent studies. However, observations of CNe and CVs, which we now identify as possible SN Ia progenitors, show that they do not spend a large amount of time at high luminosities and effective temperatures.

Moreover, some RNe are repeating sufficiently often that their WDs must have grown in mass so that they are now close to the Chandrasekhar Limit. One such system is the "rapidly recurring" RN in M31 (M31N 2008-12a) which is outbursting about once per year and has opened up a large cavity in the ISM surrounding the system ([Darnley et al. 2016, 2017a,b, 2019; Henze et al. 2015, 2018](#)). It is neither X-ray nor UV luminous between outbursts.

## 7. DISCUSSION

Fortunately for this study, the recent multi-d studies of convection in the accreted layers of WDs ([Casanova et al. 2010b,a, 2011a,b, 2016a, 2018; José 2014, and references therein](#)) implied that we could reasonably approximate their results by accreting a hydrogen-rich (solar abundances) layer and then switch to a mixed composition once the TNR was underway and convection had begun. A similar technique has already been used by [José et al. \(2007\)](#) who explored a variety of time scales for mixing the WD material into the accreted layers, once convection was underway, and found that using short time scales was warranted. We chose an "instantaneous" time for mixing both because it is reproducible and because it is not in disagreement with their results. Moreover, our initial MDTNR studies suggested that CO WDs were growing in mass and we extended our studies to  $1.35 M_{\odot}$  CO WDs.

Therefore, we have used NOVA to study the consequences of TNRs on WDs of various masses using three different compositions. In all cases we find that more mass is accreted than ejected and, therefore, the WD is growing in mass. We have used two different techniques to treat the accreting material. In the first we assumed that the solar material is mixed from the beginning of accretion (MFB). This is the technique used both by us and others in the past because there was no agreement on when and how WD material was mixed up into the accreting matter. Neither the consequences of our solar mixture accretion simulations nor those where we mix from the beginning of accretion (MFB) (Tables 1 and 2) agree with the observations of CNe outbursts.

Switching to a mixed composition once the TNR is ongoing and a major fraction of the accreted material is convective, however, provides a range of model outcomes that are more compatible with observed CNe physical parameters reported in the literature. The simulations with 25% WD matter and 75% solar matter (MDTNR) appear to fit the observations somewhat better than those with 50% WD matter and 50% solar matter (MDTNR). Nevertheless, NOVA is able to only follow one outburst and reaching to close to the Chandrasekhar Limit requires many such cycles of accretion-TNR-ejection - accretion. While this has yet to be done with either CO or ONe enriched material (this may have been done in the study of [Rukeya et al. \(2017\)](#) but they only reported their ejected mass not the accreted mass), multi-cycle evolution and the growth in mass of the WD has been done with solar accretion studies ([Starrfield 2014](#); [Hillman et al. 2015a, 2016](#); [Starrfield 2017](#)). We note that the multi-cycle studies reported in [Starrfield \(2014\)](#) and [Starrfield \(2017\)](#) were done with MESA ([Paxton et al. 2011, 2013, 2018](#), and references therein) while those described by [Hillman et al. \(2015a\)](#) and [Hillman et al. \(2016\)](#) were done with the code of [Kovetz et al. \(2009\)](#), and references therein). Given these studies with multiple codes, therefore, we feel that our single outburst result implies that the consequences of the CN outburst is the growth in mass of the WD under all situations.

Of great importance, some of the ejected isotope abundances in the simulations also fit the isotopic ratios measured for some pre-solar grains suggesting that these grains come from CNe ejecta ([Bose & Starrfield 2018](#)). [Bose & Starrfield \(2018\)](#) compared the compositions of 30 pre-solar SiC grains with the ejected isotopic abundances in Tables 5 and 6. The simulations with 25% WD matter and 75% solar matter with CO WD masses from  $0.8 M_{\odot}$  to  $1.35 M_{\odot}$  provide the best fits to the measured isotopic data in four SiC grains. In addition, one grain matches the 50% WD and 50% solar  $1.35 M_{\odot}$  MDTNR simulation. To the best of our knowledge, this is the first study that successfully applies CO nova simulations to both observations of nova dust and pre-solar grains of nova origin. Previous studies that attempted to understand SiC nova grain candidates used ONe nova simulations from [José & Hernanz \(1998\)](#), which mandated mixing >95% of solar matter with <5% of CN ejected matter to account for the grains' compositions ([Amari et al. 2001](#)). Such mixing is not required for other grain types (e.g., SiC X grains from supernovae). The other assumption, that the binary companion to the WD had to be a main sequence star, made the assignment of nova candidate grains as *bona fide* nova grains even more uncertain. However, using the simulations described here, we require less than 25% of solar system material be mixed with the CO nova ejecta to account for the grain compositions ([Bose & Starrfield 2018](#)).

Our simulations show that for CO WD mass  $\geq 1.15 M_{\odot}$  the mass fraction of  ${}^7\text{Li}$  ( ${}^7\text{Be}$ ) ejected is either  $2 \times 10^{-5}$  (25% WD matter and 75% solar matter: Table 5) or  $10^{-5}$  (50% WD matter plus 50% solar matter: Table 6). The amount of ejected mass for the same WD range is  $\sim 10^{-5} M_{\odot}$  for the 25% WD matter and 75% solar matter simulations and  $\sim 2 \times 10^{-5}$  for the 50% WD matter plus 50% solar matter simulations as given in Table 2. Interestingly, their product implies an ejected  ${}^7\text{Li}$  mass of  $\sim 2 \times 10^{-10} M_{\odot}$  for either composition. If we take a value for the CN rate of  $50 \text{ yr}^{-1}$  ([Shafter 2017](#)), a lifetime for the galaxy of  $10^{10} \text{ yr}$ , and our production values we arrive at a predicted abundance of  $\sim 100 M_{\odot}$  for the  ${}^7\text{Li}$  produced by CNe in the galaxy.

Our results confirm that CO novae are overproducing  ${}^7\text{Be}$ , which decays to  ${}^7\text{Li}$ . The amount of  ${}^7\text{Be}$  we predict from our simulations, in combination with the observations, allow us to assert that CNe are responsible for a significant fraction of the  ${}^7\text{Li}$  in the galaxy. Moreover, the observations of  ${}^7\text{Be}$  and  ${}^7\text{Li}$  found in the early high dispersion optical spectra of the ejected material from CN outbursts (both CO and ONe) ([Tajitsu et al. 2015, 2016](#); [Izzo et al. 2015, 2018](#); [Molaro et al. 2016](#); [Selvelli et al. 2018](#); [Wagner et al. 2018](#)) report much higher values than we predict. In fact, at least 10 times higher than previously predicted ([Starrfield et al. 1978](#); [Hernanz et al. 1996](#); [José & Hernanz 1998](#)).

We also address the question: *what is the total amount of  ${}^7\text{Li}$  in the galaxy?* The number usually quoted is  $\sim 150 M_{\odot}$  ([Hernanz et al. 1996](#); [Molaro et al. 2016](#)). However, we arrive at a different value. [Lodders et al. \(2009\)](#) give a value of  $2.0 \times 10^{-9}$  for the solar system abundance of  ${}^7\text{Li}/\text{H}$  by number. We convert to mass fraction by multiplying by 7 and obtain  $1.4 \times 10^{-8}$  for  $X({}^7\text{Li})/X(\text{H})$ . We assume that the total mass of the galaxy is  $\sim 10^{11} M_{\odot}$  and the mass fraction of hydrogen is 0.71 ([Lodders & Palme 2009](#); [Lodders et al. 2009](#)). Therefore, the total mass of  ${}^7\text{Li}$  in the galaxy should

be  $0.71 \times 10^{11} \times 1.4 \times 10^{-8}$  or  $\sim 1000 M_{\odot}$ . The most recent discussion of the importance of CNe for  ${}^7\text{Li}$  in the galaxy is that of [Cescutti & Molaro \(2019\)](#), and references therein) who address the discoveries of  ${}^7\text{Li}$  and  ${}^7\text{Be}$  in CN ejecta. Finally, the primordial  ${}^7\text{Li}$  abundance in the galaxy is  $\sim 80 M_{\odot}$  requiring a galactic source of  ${}^7\text{Li}$  ([Fields 2011](#)).  ${}^6\text{Li}$  is produced by spallation and not by nuclear reactions in stars, however, so that there should not be a correlation in the abundances of these two isotopes in stellar sources.

Our technique, of first accreting a solar mixture and then switching to a mixed composition, can be compared to calculations where a mixed composition was used from the beginning of the simulation ([Hernanz et al. 1996](#); [José & Hernanz 1998](#); [Rukeya et al. 2017](#)). They accreted onto both CO and ONe WDs in order to determine the  ${}^7\text{Li}$  production from CNe but did not study CO WDs as massive as in this work. They assumed two mixed compositions from the beginning (either 25% WD material or 50% WD material), with a solar ([Lodders & Palme 2009](#))  ${}^3\text{He}$  abundance of  $8.46 \times 10^{-5}$ . All our simulations used a  ${}^3\text{He}$  mass fraction ([Lodders 2003](#)) of  $3.41 \times 10^{-5}$ . Since the production of  ${}^7\text{Be}$  occurs through the  ${}^3\text{He}(\alpha, \gamma){}^7\text{Be}$  reaction, a higher abundance of  ${}^3\text{He}$  is expected to result in a higher  ${}^7\text{Be}$  abundance ([Hernanz et al. 1996](#); [José & Hernanz 1998](#)). However, the larger accreted mass in our simulations resulted both in a higher peak temperature and also stronger convection (transporting the  ${}^7\text{Be}$  more rapidly to the surface layers). These effects combined resulted in a larger amount of  ${}^7\text{Be}$  than reported in either [Hernanz et al. \(1996\)](#), [José & Hernanz \(1998\)](#), or [Rukeya et al. \(2017\)](#).

[Rukeya et al. \(2017\)](#) also compared their simulations to the total observed amount of  ${}^7\text{Li}$  in the galaxy ( $\sim 150 M_{\odot}$  given in [Hernanz et al. 1996](#)). They argued that CO novae are producing about 10% of galactic lithium. Our simulations, however, produce at least 1.5 times more  ${}^7\text{Li}$  than their simulations (or those of [José & Hernanz 1998](#)). In addition, we have also followed the  ${}^7\text{Li}$  production on more massive WDs achieving about a factor of 2 enrichment over their results. Therefore, it seems likely that CO novae can produce a significant amount of stellar  ${}^7\text{Li}$ . In [Tables 1 and 2](#) we give the ejected  ${}^7\text{Li}$  abundance in the same units as in [Hernanz et al. \(1996\)](#) so that a direct comparison can be made.

We find that the amount of *accreted* material is an inverse function of the initial abundance of  ${}^{12}\text{C}$ . Accreting solar material (rather than mixed) allows for more matter to be accreted. Reducing the metallicity to values seen in the LMC, SMC, or even lower also reduces the initial  ${}^{12}\text{C}$  allowing more material to be accreted before the TNR is initiated ([Starrfield et al. 1999](#); [José et al. 2007](#)) and the accreted material mixes with WD matter. Finally, either no mixing with the WD (RNe) or mixing too early with the CO WD (MFB) results in an outburst that ejects less material than is accreted and the WD is also growing in mass.

Finally, there is little to no observational evidence for mixing of accreted matter with WD matter in RN explosions. While all CNe are thought to be recurrent, by convention RNe are those novae that have experienced multiple recorded outbursts in the last 150 years or so. Pure solar accretion studies show that virtually no material is ejected and, therefore, those WDs must be growing rapidly in mass ([Starrfield et al. 2012a](#); [Starrfield 2014](#)).

## 8. CONCLUSIONS

1. The amount of accreted material is an inverse function of the initial abundance of  ${}^{12}\text{C}$ .
2. By first accreting solar material (rather than mixed), more matter is accreted than if we assumed mixing from the beginning. Reducing the metallicity to values in agreement with the Magellanic Clouds, or even lower, further reduces the initial  ${}^{12}\text{C}$  abundance allowing more material to be accreted before the TNR is initiated ([Starrfield et al. 1999](#); [José et al. 2007](#)).
3. Either no mixing with the WD (solar accretion) or mixing too early with the WD (MFB) results in an outburst that is less violent and little material (accreted plus WD) is ejected during the outburst. This also causes the CO WD to grow in mass. We have shown this both by following one outburst with NOVA and repeated outbursts with MESA ([Starrfield et al. 2016](#)).
4. Multi-dimensional studies show that there is sufficient mixing during the TNR to agree with observations of the ejecta abundances ([Casanova et al. 2018](#), and references therein). This mixing occurs via convective entrainment (dredge-up of WD outer layers into the accreted material) during the TNR and does not affect the total amount of accreted material since it occurs after the accretion phase of the outburst.

5. Simulations with 25% WD and 75% solar matter, mixed after the TNR is underway, eject only a fraction of the accreted material. Therefore, the WD is *growing* in mass as a result of the Classical Nova phenomena (see Figure 8).
6. Simulations with 50% WD and 50% solar matter, mixed after the TNR is underway, ejected a larger fraction of accreted material but not as much as was accreted. Therefore, these simulations, with more  $^{12}\text{C}$ , also imply that the WD is growing in mass as a result of the Classical Nova phenomena. They also reached higher peak temperatures and ejected more material moving at higher velocities than those with only 25% WD and 75% solar matter.
7. Our simulations confirm that CO novae are overproducing  $^7\text{Be}$ , which decays to  $^7\text{Li}$  after we have ended our simulations. This result is in agreement with the observations of enriched  $^7\text{Be}$  in CN explosions, although the observed values exceed our predictions and those of others.
8. Our simulations show that the analyses of Nomoto (1982) and (Fujimoto 1982a,b) are not supported by modern evolutionary or hydrodynamic simulations and that, by themselves, do not argue against the single degenerate scenario for SN Ia progenitors.
9. While we do not rule out the SSS as SN Ia progenitors, their observed numbers suggest that they are likely to be an extremely small channel with typical CVs being a major channel. Finally, the observations of SN Ia explosions alone suggest that there are multiple channels for their progenitors (Polin et al. 2019, and references therein).
10. Our results indicate that even systems with low accretion rates,  $\dot{M} < 10^{-9} M_{\odot} \text{ yr}^{-1}$ , can produce CNe in which the WD is growing in mass toward the Chandrasekhar Limit. In combination with the results of Hillman et al. (2015b, 2016, done with a different code and higher mass accretion rates), our simulations add a considerable area to the  $\dot{M}$  - WD mass plane, where evolution to a SN Ia is possible. It is no longer necessary to assume that the only area in which the WD grows in mass is that region designated as the “Steady Burning” region.

We acknowledge useful discussion and encouragement from M. Darnley, E. Aydi, J. José, M. Hernanz, A. Heger, S. Kafka, L. Izzo, P. Molaro, M. della Valle, A. Shafter and the attendees at EWASS18, COSPAR 2018, and HEAD 2019 for their comments. We thank the anonymous referee, J. José, and A. Shafter for their comments on an earlier draft which greatly improved this manuscript. This work was supported in part by NASA under the Astrophysics Theory Program grant 14-ATP14-0007 and the U.S. DOE under Contract No. DE-FG02-97ER41041. SS acknowledges partial support from NASA, NSF and HST grants to ASU, WRH is supported by the U.S. Department of Energy, Office of Nuclear Physics, and CEW acknowledges support from NASA and NSF.

## REFERENCES

- Althaus, L. G., Córscico, A. H., Bischoff-Kim, A., et al. 2010, *Astrophys. J.*, 717, 897, doi: [10.1088/0004-637X/717/2/897](https://doi.org/10.1088/0004-637X/717/2/897)
- Amari, S., Gao, X., Nittler, L. R., et al. 2001, *Astrophys. J.*, 551, 1065, doi: [10.1086/320235](https://doi.org/10.1086/320235)
- Anders, E., & Grevesse, N. 1989, *GeoCoA*, 53, 197
- Arnett, D., Meakin, C., & Young, P. A. 2010, *Astrophys. J.*, 710, 1619, doi: [10.1088/0004-637X/710/2/1619](https://doi.org/10.1088/0004-637X/710/2/1619)
- Bahcall, J. N., & Moeller, C. P. 1969, *Astrophys. J.*, 155, 511, doi: [10.1086/149887](https://doi.org/10.1086/149887)
- Bode, M. F., & Evans, A. 2008, *Classical Novae*, 2nd edn. (Cambridge: University Press)
- Bose, M., & Starrfield, S. 2018, arXiv e-prints. <https://arxiv.org/abs/1812.11432>
- Branch, D., Livio, M., Yungelson, L. R., Boffi, F. R., & Baron, E. 1995, *PASP*, 107, 1019, doi: [10.1086/133657](https://doi.org/10.1086/133657)
- Cameron, A. G. W., & Fowler, W. A. 1971, *Astrophys. J.*, 164, 111, doi: [10.1086/150821](https://doi.org/10.1086/150821)
- Casanova, J., José, J., García-Berro, E., Calder, A., & Shore, S. N. 2010a, *Astron. Astrophys.*, 513, L5, doi: [10.1051/0004-6361/201014178](https://doi.org/10.1051/0004-6361/201014178)
- . 2010b, *Astron. Astrophys.*, 513, L5+, doi: [10.1051/0004-6361/201014178](https://doi.org/10.1051/0004-6361/201014178)
- . 2011a, *Astron. Astrophys.*, 527, A5, doi: [10.1051/0004-6361/201015895](https://doi.org/10.1051/0004-6361/201015895)

- Casanova, J., Jose, J., Garcia-Berro, E., & Shore, S. N. 2016a, ArXiv e-prints. <https://arxiv.org/abs/1606.08734>
- Casanova, J., José, J., García-Berro, E., & Shore, S. N. 2016b, *Astron. Astrophys.*, 595, A28, doi: [10.1051/0004-6361/201628707](https://doi.org/10.1051/0004-6361/201628707)
- Casanova, J., José, J., García-Berro, E., Shore, S. N., & Calder, A. C. 2011b, *Nature*, 478, 490, doi: [10.1038/nature10520](https://doi.org/10.1038/nature10520)
- Casanova, J., Jose, J., & Shore, S. N. 2018, ArXiv e-prints. <https://arxiv.org/abs/1807.10646>
- Cassisi, S., Potekhin, A. Y., Pietrinferni, A., Catelan, M., & Salari, M. 2007, *Astrophys. J.*, 661, 1094
- Cescutti, G., & Molaro, P. 2019, *Mon. Not. R. Astron. Soc.*, 482, 4372, doi: [10.1093/mnras/sty2967](https://doi.org/10.1093/mnras/sty2967)
- Copperwheat, C. M., Marsh, T. R., Dhillon, V. S., et al. 2010, *Mon. Not. R. Astron. Soc.*, 402, 1824, doi: [10.1111/j.1365-2966.2009.16010.x](https://doi.org/10.1111/j.1365-2966.2009.16010.x)
- Cowley, A. P., Schmidtke, P. C., Crampton, D., & Hutchings, J. B. 1998, *Astrophys. J.*, 504, 854, doi: [10.1086/306123](https://doi.org/10.1086/306123)
- Darnley, M. J., Henze, M., Bode, M. F., et al. 2016, eprint ArXiv -1607.08082. <https://arxiv.org/abs/1607.08082>
- Darnley, M. J., Hounsell, R., Godon, P., et al. 2017a, *Astrophys. J.*, 847, 35, doi: [10.3847/1538-4357/aa8867](https://doi.org/10.3847/1538-4357/aa8867)
- . 2017b, *Astrophys. J.*, 849, 96, doi: [10.3847/1538-4357/aa9062](https://doi.org/10.3847/1538-4357/aa9062)
- Darnley, M. J., Hounsell, R., O'Brien, T. J., et al. 2019, *Nature*, 565, 460, doi: [10.1038/s41586-018-0825-4](https://doi.org/10.1038/s41586-018-0825-4)
- Downen, L., Iliadis, C., Jose, J., & Starrfield, S. 2012, in *Nuclei in the Cosmos (NIC XII)*, Vol. Online only
- Echevarría, J., de la Fuente, E., & Costero, R. 2007, *Astron. J.*, 134, 262, doi: [10.1086/518562](https://doi.org/10.1086/518562)
- Fields, B. D. 2011, *Annual Review of Nuclear and Particle Science*, 61, 47, doi: [10.1146/annurev-nucl-102010-130445](https://doi.org/10.1146/annurev-nucl-102010-130445)
- Fujimoto, M. Y. 1982a, *Astrophys. J.*, 257, 752, doi: [10.1086/160029](https://doi.org/10.1086/160029)
- . 1982b, *Astrophys. J.*, 257, 767, doi: [10.1086/160030](https://doi.org/10.1086/160030)
- Gehrz, R. D., Truran, J. W., Williams, R. E., & Starrfield, S. 1998, *PASP*, 110, 3
- Giammichele, N., Charpinet, S., Fontaine, G., et al. 2018, *Nature*, 554, 73, doi: [10.1038/nature25136](https://doi.org/10.1038/nature25136)
- Gilfanov, M., & Bogdán, Á. 2010, *Nature*, 463, 924, doi: [10.1038/nature08685](https://doi.org/10.1038/nature08685)
- Graur, O., & Woods, T. E. 2019, *Mon. Not. R. Astron. Soc.*, 484, L79, doi: [10.1093/mnrasl/slz005](https://doi.org/10.1093/mnrasl/slz005)
- Henze, M., Darnley, M. J., Kabashima, F., et al. 2015, *Astron. Astrophys.*, 582, L8, doi: [10.1051/0004-6361/201527168](https://doi.org/10.1051/0004-6361/201527168)
- Henze, M., Darnley, M. J., Williams, S. C., et al. 2018, *Astrophys. J.*, 857, 68, doi: [10.3847/1538-4357/aab6a6](https://doi.org/10.3847/1538-4357/aab6a6)
- Hernanz, M. 2015, *Nature*, 518, 307, doi: [10.1038/518307a](https://doi.org/10.1038/518307a)
- Hernanz, M., Jose, J., Coc, A., & Isern, J. 1996, *Astrophys. J.*, 465, L27, doi: [10.1086/310122](https://doi.org/10.1086/310122)
- Hillebrandt, W., & Niemeyer, J. C. 2000, *ARA&A*, 38, 191
- Hillman, Y., Prialnik, D., Kovetz, A., & Shara, M. M. 2015a, ArXiv e-prints. <https://arxiv.org/abs/1508.03141>
- . 2015b, *Mon. Not. R. Astron. Soc.*, 446, 1924, doi: [10.1093/mnras/stu2235](https://doi.org/10.1093/mnras/stu2235)
- . 2016, *Astrophys. J.*, 819, 168, doi: [10.3847/0004-637X/819/2/168](https://doi.org/10.3847/0004-637X/819/2/168)
- Hillman, Y., Prialnik, D., Kovetz, A., Shara, M. M., & Neill, J. D. 2014, *Mon. Not. R. Astron. Soc.*, 437, 1962, doi: [10.1093/mnras/stt2027](https://doi.org/10.1093/mnras/stt2027)
- Hix, W. R., & Thielemann, F.-K. 1999, *Astrophys. J.*, 511, 862, doi: [10.1086/306692](https://doi.org/10.1086/306692)
- Iben, Jr., I. 1991, *ApJS*, 76, 55, doi: [10.1086/191565](https://doi.org/10.1086/191565)
- Iben, Icko, J., Ritossa, C., & García-Berro, E. 1997, *Astrophys. J.*, 489, 772, doi: [10.1086/304822](https://doi.org/10.1086/304822)
- Iglesias, C. A., & Rogers, F. J. 1993, *Astrophys. J.*, 412, 752, doi: [10.1086/172958](https://doi.org/10.1086/172958)
- . 1996, *Astrophys. J.*, 464, 943
- Izzo, L., Della Valle, M., Mason, E., et al. 2015, *Astrophys. J.*, 808, L14, doi: [10.1088/2041-8205/808/1/L14](https://doi.org/10.1088/2041-8205/808/1/L14)
- Izzo, L., Molaro, P., Bonifacio, P., et al. 2018, *Mon. Not. R. Astron. Soc.*, doi: [10.1093/mnras/sty435](https://doi.org/10.1093/mnras/sty435)
- José, J. 2014, in *Astronomical Society of the Pacific Conference Series*, Vol. 490, *Stella Novae: Past and Future Decades*, ed. P. A. Woudt & V. A. R. M. Ribeiro, 275
- José, J., García-Berro, E., Hernanz, M., & Gil-Pons, P. 2007, *Astrophys. J.*, 662, L103
- José, J., Halabi, G. M., & El Eid, M. F. 2016, *Astron. Astrophys.*, 593, A54, doi: [10.1051/0004-6361/201628901](https://doi.org/10.1051/0004-6361/201628901)
- José, J., & Hernanz, M. 1998, *Astrophys. J.*, 494, 680, doi: [10.1086/305244](https://doi.org/10.1086/305244)
- Kahabka, P., & van den Heuvel, E. P. J. 1997, *ARA&A*, 35, 69, doi: [10.1146/annurev.astro.35.1.69](https://doi.org/10.1146/annurev.astro.35.1.69)
- Kasliwal, M. M., Cenko, S. B., Kulkarni, S. R., et al. 2011, *Astrophys. J.*, 735, 94, doi: [10.1088/0004-637X/735/2/94](https://doi.org/10.1088/0004-637X/735/2/94)
- Kelly, K. J., Iliadis, C., Downen, L., José, J., & Champagne, A. 2013, *Astrophys. J.*, 777, 130, doi: [10.1088/0004-637X/777/2/130](https://doi.org/10.1088/0004-637X/777/2/130)
- Kovetz, A., Yaron, O., & Prialnik, D. 2009, *Mon. Not. R. Astron. Soc.*, 395, 1857, doi: [10.1111/j.1365-2966.2009.14670.x](https://doi.org/10.1111/j.1365-2966.2009.14670.x)

- Kutter, G. S., & Sparks, W. M. 1972, *Astrophys. J.*, 175, 407, doi: [10.1086/151567](https://doi.org/10.1086/151567)
- . 1974, *Astrophys. J.*, 192, 447, doi: [10.1086/153076](https://doi.org/10.1086/153076)
- . 1980, *Astrophys. J.*, 239, 988, doi: [10.1086/158187](https://doi.org/10.1086/158187)
- Kuuttila, J., Gilfanov, M., Seitenzahl, I. R., Woods, T. E., & Vogt, F. P. A. 2019, *Mon. Not. R. Astron. Soc.*, 484, 1317, doi: [10.1093/mnras/stz065](https://doi.org/10.1093/mnras/stz065)
- Leibundgut, B. 2000, *A&A Rv*, 10, 179, doi: [10.1007/s001590000009](https://doi.org/10.1007/s001590000009)
- . 2001, *ARA&A*, 39, 67
- Lodders, K. 2003, *Astrophys. J.*, 591, 1220
- Lodders, K., & Palme, H. 2009, *Meteoritics and Planetary Science Supplement*, 72, 5154
- Lodders, K., Palme, H., & Gail, H.-P. 2009, *Landolt Börnstein*, 712, doi: [10.1007/978-3-540-88055-4\\_34](https://doi.org/10.1007/978-3-540-88055-4_34)
- MacDonald, J. 1980, *Mon. Not. R. Astron. Soc.*, 191, 933, doi: [10.1093/mnras/191.4.933](https://doi.org/10.1093/mnras/191.4.933)
- Maoz, D., Mannucci, F., & Nelemans, G. 2014, *ARA&A*, 52, 107, doi: [10.1146/annurev-astro-082812-141031](https://doi.org/10.1146/annurev-astro-082812-141031)
- Molaro, P., Izzo, L., Mason, E., Bonifacio, P., & Della Valle, M. 2016, *Mon. Not. R. Astron. Soc.*, 463, L117, doi: [10.1093/mnrasl/slw169](https://doi.org/10.1093/mnrasl/slw169)
- Newsham, G., Starrfield, S., & Timmes, F. X. 2014, in *Astronomical Society of the Pacific Conference Series*, Vol. 490, *Stella Novae: Past and Future Decades*, ed. P. A. Woudt & V. A. R. M. Ribeiro, 287
- Nomoto, K. 1982, *Astrophys. J.*, 253, 798, doi: [10.1086/159682](https://doi.org/10.1086/159682)
- Orio, M., Ness, J.-U., Dobrotka, A., et al. 2018, *Astrophys. J.*, 862, 164, doi: [10.3847/1538-4357/aacf06](https://doi.org/10.3847/1538-4357/aacf06)
- Paxton, B., Bildsten, L., Dotter, A., et al. 2011, *ApJS*, 192, 3, doi: [10.1088/0067-0049/192/1/3](https://doi.org/10.1088/0067-0049/192/1/3)
- Paxton, B., Cantiello, M., Arras, P., et al. 2013, *ApJS*, 208, 4, doi: [10.1088/0067-0049/208/1/4](https://doi.org/10.1088/0067-0049/208/1/4)
- Paxton, B., Marchant, P., Schwab, J., et al. 2015, *ApJS*, 220, 15, doi: [10.1088/0067-0049/220/1/15](https://doi.org/10.1088/0067-0049/220/1/15)
- . 2016, *ApJS*, 223, 18, doi: [10.3847/0067-0049/223/1/18](https://doi.org/10.3847/0067-0049/223/1/18)
- Paxton, B., Schwab, J., Bauer, E. B., et al. 2018, *ApJS*, 234, 34, doi: [10.3847/1538-4365/aaa5a8](https://doi.org/10.3847/1538-4365/aaa5a8)
- Perlmutter, S., Aldering, G., Goldhaber, G., et al. 1999, *Astrophys. J.*, 517, 565, doi: [10.1086/307221](https://doi.org/10.1086/307221)
- Polin, A., Nugent, P., & Kasen, D. 2019, *Astrophys. J.*, 873, 84, doi: [10.3847/1538-4357/aafb6a](https://doi.org/10.3847/1538-4357/aafb6a)
- Riess, A. G., Filippenko, A. V., Challis, P., et al. 1998, *Astron. J.*, 116, 1009, doi: [10.1086/300499](https://doi.org/10.1086/300499)
- Ritossa, C., Garcia-Berro, E., & Iben, Jr., I. 1996, *Astrophys. J.*, 460, 489, doi: [10.1086/176987](https://doi.org/10.1086/176987)
- Ruiz-Lapuente, P. 2014, *New Astronomy Reviews*, 62, 15, doi: [10.1016/j.newar.2014.08.002](https://doi.org/10.1016/j.newar.2014.08.002)
- Rukeya, R., Lü, G., Wang, Z., & Zhu, C. 2017, *PASP*, 129, 074201, doi: [10.1088/1538-3873/aa6b4d](https://doi.org/10.1088/1538-3873/aa6b4d)
- Sallaska, A. L., Iliadis, C., Champagne, A. E., et al. 2013, *ApJS*, 207, 18. <https://arxiv.org/abs/1304.7811>
- Schwarz, G. J., Shore, S. N., Starrfield, S., et al. 2001, *Mon. Not. R. Astron. Soc.*, 320, 103, doi: [10.1046/j.1365-8711.2001.03960.x](https://doi.org/10.1046/j.1365-8711.2001.03960.x)
- Schwarzschild, M., & Härm, R. 1965, *Astrophys. J.*, 142, 855, doi: [10.1086/148358](https://doi.org/10.1086/148358)
- Selvelli, P., & Gilmozzi, R. 2019, *Astron. Astrophys.*, 622, A186, doi: [10.1051/0004-6361/201834238](https://doi.org/10.1051/0004-6361/201834238)
- Selvelli, P., Molaro, P., & Izzo, L. 2018, *Mon. Not. R. Astron. Soc.*, 481, 2261, doi: [10.1093/mnras/sty2310](https://doi.org/10.1093/mnras/sty2310)
- Shafter, A. W. 1983, PhD thesis, California Univ., Los Angeles.
- . 2017, *Astrophys. J.*, 834, 196, doi: [10.3847/1538-4357/834/2/196](https://doi.org/10.3847/1538-4357/834/2/196)
- Shara, M. M., Prialnik, D., Hillman, Y., & Kovetz, A. 2018, *Astrophys. J.*, 860, 110, doi: [10.3847/1538-4357/aabfbd](https://doi.org/10.3847/1538-4357/aabfbd)
- Sion, E. M. 1986, *Publications of the Astronomical Society of the Pacific*, 98, 821, doi: [10.1086/131831](https://doi.org/10.1086/131831)
- Sion, E. M., Godon, P., Myzcka, J., & Blair, W. P. 2010, *Astrophys. J.*, 716, L157, doi: [10.1088/2041-8205/716/2/L157](https://doi.org/10.1088/2041-8205/716/2/L157)
- Sion, E. M., Wilson, R. E., Godon, P., et al. 2018, arXiv e-prints. <https://arxiv.org/abs/1812.09993>
- Sparks, W. M., & Kutter, G. S. 1972, *Astrophys. J.*, 175, 707, doi: [10.1086/151592](https://doi.org/10.1086/151592)
- Starrfield, S. 1989, in *Classical Novae*, ed. M. F. Bode & A. Evans, 39–60
- Starrfield, S. 2014, *AIP Advances*, 4, 041007, doi: [10.1063/1.4866984](https://doi.org/10.1063/1.4866984)
- . 2017, *Evolution of Accreting White Dwarfs to the Thermonuclear Runaway*, ed. A. W. Alsabti & P. Murdin (Springer Berlin / Heidelberg), 1211
- Starrfield, S., Gehrz, R. D., & Truran, J. W. 1997, in *American Institute of Physics Conference Series*, Vol. 402, *Astrophysical implications of the laboratory study of presolar materials*, ed. E. K. Zinner & T. J. Bernatowicz, 203–234
- Starrfield, S., Iliadis, C., & Hix, W. R. 2016, *PASP*, 128, 051001, doi: [10.1088/1538-3873/128/963/051001](https://doi.org/10.1088/1538-3873/128/963/051001)
- Starrfield, S., Iliadis, C., Hix, W. R., Timmes, F. X., & Sparks, W. M. 2009, *Astrophys. J.*, 692, 1532, doi: [10.1088/0004-637X/692/2/1532](https://doi.org/10.1088/0004-637X/692/2/1532)
- Starrfield, S., Iliadis, C., Timmes, F. X., et al. 2012a, *Bulletin of the Astronomical Society of India*, 40, 419. <https://arxiv.org/abs/1210.6086>

- Starrfield, S., Schwarz, G. J., Truran, J. W., & Sparks, W. M. 1999, in *Bulletin of the American Astronomical Society*, Vol. 31, American Astronomical Society Meeting Abstracts #194, 977
- Starrfield, S., Timmes, F. X., Iliadis, C., et al. 2012b, *Baltic Astronomy*, 21, 76. <https://arxiv.org/abs/1211.6145>
- Starrfield, S., Truran, J. W., Sparks, W. M., & Arnould, M. 1978, *Astrophys. J.*, 222, 600, doi: [10.1086/156175](https://doi.org/10.1086/156175)
- Starrfield, S., Truran, J. W., Sparks, W. M., & Kutter, G. S. 1972, *Astrophys. J.*, 176, 169, doi: [10.1086/151619](https://doi.org/10.1086/151619)
- Tajitsu, A., Sadakane, K., Naito, H., Arai, A., & Aoki, W. 2015, *Nature*, 518, 381, doi: [10.1038/nature14161](https://doi.org/10.1038/nature14161)
- Tajitsu, A., Sadakane, K., Naito, H., et al. 2016, *Astrophys. J.*, 818, 191, doi: [10.3847/0004-637X/818/2/191](https://doi.org/10.3847/0004-637X/818/2/191)
- Timmes, F. X., & Arnett, D. 1999, *ApJS*, 125, 277
- Timmes, F. X., & Swesty, F. D. 2000, *ApJS*, 126, 501
- Timmes, F. X., Woosley, S. E., & Weaver, T. A. 1995, *ApJS*, 98, 617
- Trümper, J., Hasinger, G., Aschenbach, B., et al. 1991, *Nature*, 349, 579, doi: [10.1038/349579a0](https://doi.org/10.1038/349579a0)
- van den Heuvel, E. P. J., Bhattacharya, D., Nomoto, K., & Rappaport, S. A. 1992, *Astron. Astrophys.*, 262, 97
- Wagner, R. M., Woodward, C. E., Starrfield, S., Ilyin, I., & Strassmeier, K. 2018, in *American Astronomical Society Meeting Abstracts*, Vol. 231, American Astronomical Society Meeting Abstracts #231, 358.10
- Warner, B. 1995, *Cataclysmic Variable Stars.*, Vol. 28 (Cambridge University Press), 572
- Yaron, O., Prialnik, D., Shara, M. M., & Kovetz, A. 2005, *Astrophys. J.*, 623, 398, doi: [10.1086/428435](https://doi.org/10.1086/428435)
- Yoon, S.-C., Langer, N., & van der Sluys, M. 2004, *Astron. Astrophys.*, 425, 207, doi: [10.1051/0004-6361:20040231](https://doi.org/10.1051/0004-6361:20040231)